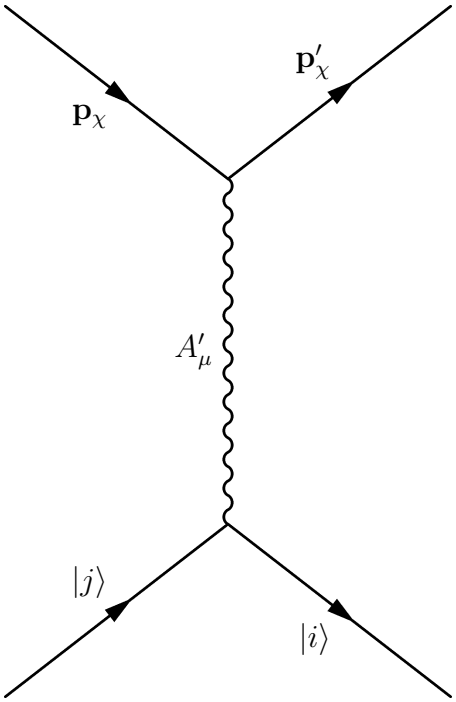

Dark Matter Interactions with Sun-like Celestial Bodies

An Exploration of How Sub-GeV Dark Matter Could Interact with Solar-like Media Through Linear Response Theory

Master's thesis in Physics

GUSTAV STRANDLYCKE

DEPARTMENT OF PHYSICS

CHALMERS UNIVERSITY OF TECHNOLOGY
Gothenburg, Sweden 2024
www.chalmers.se

Master's thesis 2024

Dark Matter Interactions with Sun-like Celestial Bodies

An Exploration of How Sub-GeV Dark Matter Could Interact with Solar-like Media Through Linear Response Theory

GUSTAV STRANDLYCKE

CHALMERS
UNIVERSITY OF TECHNOLOGY

Department of Physics
Division of Subatomic and High Energy Physics
Chalmers University of Technology
Gothenburg, Sweden 2024

Dark Matter Interactions with Sun-like Celestial Bodies
An Exploration of How Sub-GeV Dark Matter Could Interact with Solar-like Media Through Linear Response Theory
GUSTAV STRANDLYCKE

Supervisor: Riccardo Catena, Department of Physics
Examiner: Riccardo Catena, Department of Physics

Master's Thesis 2024
Department of Physics
Division of Subatomic and High Energy Physics
Chalmers University of Technology
SE-412 96 Gothenburg
Telephone +46 31 772 1000

Acknowledgements, dedications, and similar personal statements in this +thesis, reflect the author's own views.

Cover: Feynman diagram of the studied process showing a dark matter particle, χ, interacting with the electrons of the medium via a heavy dark photon, A'_μ.

Typeset in LaTeX
Printed by Chalmers Reproservice
Gothenburg, Sweden 2024

Dark Matter Interactions with Sun-like Celestial Bodies
An Exploration of How Sub-GeV Dark Matter Could Interact with Solar-like Media Through Linear Response Theory

GUSTAV STRANDLYCKE
Department of Physics
Chalmers University of Technology

Abstract

One interesting avenue in the search for dark matter is the possibility of dark matter interacting with celestial bodies, like our Sun, in such a way that the effects can be detected here on Earth. The purpose of this thesis is to investigate how sub-GeV Dirac-type dark matter particles could interact with the electrons in the Sun via a heavy dark photon. This study also aims to account for the surrounding medium and its effects on these scattering rates, Γ, through in-medium effects using the framework of linear response theory, specifically the density-density response function, $\chi_{\rho\rho}$. The impact of the medium will be demonstrated by comparing the scattering rates calculated through linear response theory to those calculated without considering the medium. Using these calculated scattering rates, in both the heavy and light mediator limits, the resulting dark matter capture rates, C, inside the Sun, for various dark matter masses, m_χ, and dark matter-electron reference cross sections, $\bar{\sigma}_e$, are calculated. Furthermore, the calculated scattering rates are applied to the phenomenon of solar dark matter reflection where in-medium effects are also demonstrated to be of some importance.

Keywords: dark matter, dark photon, sub-GeV, in-medium effects, linear response theory, scattering rates, dark matter capture, dark matter reflection

Acknowledgements

I would like to thank my supervisor Riccardo Catena who has helped me throughout this Master's project by giving me invaluable guidance. Furthermore, I would like to thank my fellow Master's students Eli Ismailov, Thomas Jerkvall and Andreas Lund who have helped me stay somewhat sane through the means of valuable discussions. Last but not least I would also like to thank my family.

Gustav Strandlycke, Gothenburg, June 2024

List of Acronyms

Below is the list of acronyms that have been used throughout this thesis listed in alphabetical order:

EFT	Effective Field Theory
QED	Quantum Electrodynamics
RPA	Random Phase Approximation
WIMP	Weakly Interacting Massive Particle
1PI	One Particle Irreducible

Nomenclature

Below is the nomenclature of indices, particles, operators, functions and variables that have been used throughout this thesis.

Indices

j	Index for incoming electron state
i	Index for outgoing electron state
s, s'	Spin number for incoming and outgoing dark matter particle

Particles

χ	(Relativistic) dark matter particle
ψ_χ	Non-relativistic wave function for dark matter particle
A'_μ	Dark photon
A_μ	Photon
e	(Relativistic) electron
ψ_e	Non-relativistic wave function for electron

Operators

$\mathcal{L}$	Lagrangian density
$\hat{a}_{s\mathbf{p}}$	Annihilation operator for mode with spin number s and momentum $\mathbf{p}$
$\hat{a}^\dagger_{s\mathbf{p}}$	Creation operator for mode with spin number s and momentum $\mathbf{p}$
H_0	Hamiltonian of unperturbed system
ρ_e	Density operator of electrons

Functions

$i\mathcal{M}_{j\to i}$	Feynman amplitude of channel from initial state j to final state i
σ	Cross section
S	Dynamical structure factor
$\chi_{\rho\rho}$	Density-density response function
Π_e, Π_N	1 particle irreducible for electron and ion respectively
V_e	Coulomb interaction
$f_{\mathbf{p}}$	Occupation number at momentum, $\mathbf{p}$
ε	Dielectric function
Γ	Scattering rate
C	Capture rate

Variables

$\mathbf{p}_\chi$	Incoming dark matter momentum
$\mathbf{p}'_\chi$	Outgoing dark matter momentum
Q	Transferred momentum
ω	Transferred energy
e	Electric charge
g_χ, g_e	Coupling constants to dark photon for dark matter particle and electron
m_e, m_χ, m'_A	Mass for electron, dark matter particle and dark photon
$\mu_{\chi e}$	Reduced mass of electron and dark matter pair
v_χ	(Initial) dark matter velocity
α	Quantum electrodynamics fine structure constant
$\bar{\sigma}_e$	Reference cross section between dark matter particle and electron
T	Temperature
β	Inverse temperature
n_e, n_{H}, n_{He}	Number densities for electrons, hydrogen and helium
Z	Atomic charge number
n_χ	Number density for halo dark matter particles
v_{esc}	Escape velocity
$M_\odot$	Mass of the Sun

v_0	Velocity dispersion of halo dark matter
v_*	Velocity of the Sun relative to the Milky Way
J	Angular momentum

Contents

List of Figures

List of Tables

1

Introduction

In the vast tapestry of the cosmos, the mystery of dark matter stands as one of the most compelling enigmas of modern astro- and particle physics. For decades, astronomers and particle physicists have grappled with the profound implications of a substance that eludes direct detection yet exerts an observable gravitational influence. The quest to understand dark matter transcends mere academic curiosity, as it could hold the key to unravelling fundamental concepts of the universe and its evolution.

To introduce the subject of dark matter, we will, in this first chapter, provide a brief background to the field. Presenting some of the observational evidence for it, along with theoretically proposed dark matter candidates and experimental approaches aimed at detecting it. With this background in place, we will then specify the focus and purpose of this thesis before also giving an overview of its structure. Throughout this thesis, natural units will be assumed, meaning $\hbar = c = k_B = 1$.

1.1 Background

The story of dark matter unfolds against the backdrop of a rich history marked by groundbreaking discoveries and paradigm-shifting revelations [1, 2]. It finds its roots in the early 20th century, when pioneering astronomers such as Fritz Zwicky observed peculiar dynamics within galaxy clusters [3]. Zwicky's investigations into the velocities of galaxies within the Coma Cluster hinted at the presence of unseen mass, leading him to postulate the existence of dark matter. This hypothesis laid the groundwork for future explorations into the nature of cosmic mass.

However, it was in the 1970s that the field of dark matter studies really started to gain momentum. Through observations of the rotational velocities of stars within spiral galaxies, several articles demonstrated the property of flat rotation curves for spiral galaxies. It was seen that the rotational velocity of spiral galaxies is roughly constant as a function of the distance from the centre of the galaxy (see, for example, Refs. [4–6]). These results contradicted the expectation of decaying rotational velocity, which would be the case for spiral galaxies containing only the previously observed luminous matter. This discrepancy between observed rotational

velocities and those predicted by visible matter alone pointed towards the existence of a vast reservoir of unseen mass distributed throughout galaxies, providing crucial support for the dark matter hypothesis (see, for example, Refs. [7–9]).

Since these pioneering observations, a wealth of evidence has further supported the case for dark matter. Additional observational evidence includes the nature of the cosmic microwave background radiation [10–12], the large-scale structure of the universe [13], the results of gravitational lensing experiments [14], and the way galaxy clusters merge [15].

In the pursuit of unravelling the mystery of dark matter, scientists have explored a myriad of theoretical and observational avenues, leading to the formulation of various dark matter candidates. These candidates span a diverse spectrum of particles and phenomena, each offering unique insights into the elusive nature of cosmic mass [1, 2].

One of the most prominent dark matter candidates is the Weakly Interacting Massive Particle (WIMP). Proposed in the 1980s within the framework of supersymmetric extensions to the Standard Model of particle physics, WIMPs possess several attractive properties that make them compelling candidates for dark matter [16]. Notably, their weak-scale interactions would naturally explain the observed relic abundance of dark matter in the universe, as inferred from cosmological observations [17–19]. Additionally, WIMPs feature prominently in many theoretical models aimed at addressing the hierarchy problem and unifying fundamental forces [20].

Another notable dark matter candidate is the axion. Originally proposed to solve the strong CP problem in quantum chromodynamics [21–24], axions were soon constrained to be light and feebly interacting [25–27]. These properties have interesting cosmological consequences, and due to axions being stable over cosmological timescales, they could constitute dark matter if enough were produced in the early universe [28–32].

Additional dark matter candidates include sterile neutrinos and primordial black holes. Sterile neutrinos, hypothesised to exist outside the framework of the Standard Model, possess properties that make them viable dark matter candidates [33]. Their interactions are weaker than those of standard model neutrinos, and they could have masses on the order of keV. Primordial black holes, formed in the dense conditions of the early universe, represent another intriguing possibility for dark matter, offering a unique window into the primordial universe and its cosmological evolution [34–36].

Alternative theoretical frameworks, beyond particle-based dark matter candidates, such as modified gravity theories, have been proposed to explain the observed gravitational phenomena attributed to dark matter [37–39]. These theories seek to modify the laws of gravity on cosmic scales, offering an alternative explanation for the observed dynamics of galaxies and galaxy clusters without introducing exotic particles [40].

The exploration of dark matter candidates represents a multifaceted endeavour consisting of both thorough theoretical speculation and experimental ingenuity. While significant progress has been made in elucidating the properties of dark matter candidates, the quest for a definitive understanding of cosmic mass remains ongoing, driving continued innovation at the forefront of astro- and particle physics [1].

Moving on from theoretical speculation, the quest to unveil the nature of dark matter has spurred an array of experimental efforts aimed at detecting and characterising its constituents. These experimental endeavours span a wide range of techniques, from searching for dark matter particles in particle colliders to deploying sophisticated detectors deep underground and scrutinising the cosmos for indirect signatures of dark matter annihilation, decay, or interactions [1].

Particle colliders, such as the Large Hadron Collider (LHC) at CERN, represent one avenue for exploring the properties of dark matter candidates through high-energy particle collisions. By smashing protons or other particles together at near-light speeds, these experiments aim to create dark matter particles that can then be detected. One type of particle that could potentially be observed with the help of a particle collider is the WIMP [41, 42].

Indirect detection methods offer another avenue for uncovering the presence of dark matter by searching for secondary signatures of dark matter annihilation or decay in the cosmos [1]. These methods involve observing high-energy particles, such as gamma rays, neutrinos, or cosmic rays, produced as a result of dark matter interactions in regions of high dark matter density, such as the halo of our galaxy or within the Sun where dark matter could have been gravitationally captured [43, 44]. This will also be investigated further in this thesis. By analysing the spatial and spectral characteristics of these secondary particles, indirect detection experiments seek to infer the presence and properties of dark matter particles, providing complementary insights to direct detection efforts.

Direct detection experiments aim to detect the rare interactions between dark matter particles and ordinary matter within sensitive detectors here on Earth. These experiments typically utilise detectors based on technologies such as semiconductor materials to search for the faint signals generated by dark matter scattering off atomic nuclei or, for lighter, sub-GeV dark matter, scatterings between dark matter and electrons [1, 45]. Some of these experiments focusing on sub-GeV dark matter, which is the mass range that will also be the focus of this report, include SENSEI [46], DAMIC [47], SuperCDMS [48], CDEX [49], and EDELWEISS [50].

To summarise the vast field of dark matter-related astro- and particle physics, there is compelling evidence suggesting the existence of a substance that falls under the umbrella of dark matter. Due to its elusive nature, numerous theories attempt to explain its properties, and numerous experiments aim to observe it. Since experiments have yet to successfully observe signals that can be definitively attributed to dark matter, the search continues. It is against this backdrop that this thesis aims

to contribute by focusing on how sub-GeV dark matter could interact primarily with the electrons in the Sun since this could be important both for direct and indirect detection experiments.

1.2 Purpose

The purpose of this thesis is to investigate how the sub-GeV mass range of dark matter Dirac-type particles interact with electrons in the Sun via a massive dark photon. We consider in-medium effects within the framework of linear response theory using the formalism of Ref. [45]. Utilising the results of these calculations, the aim is to apply them to the formalism behind dark matter capture in celestial bodies as outlined in Ref. [51] and to the phenomenon of solar reflection as discussed in Ref. [52].

1.3 Structure of Thesis

This thesis will begin with the necessary calculations to obtain the scattering rate of the dark matter particle in the solar medium in Chapter 2. Following this, we will describe the concepts needed for dark matter capture in Chapter 3 and dark matter reflections in Chapter 4. Additionally, Appendices A and B provide an introduction to the field of linear response theory and explain how the density-density response function relates to the dielectric function. Appendix C presents the solar model used in this thesis.

2

Scattering Rate of Dark Matter with Electrons in a Solar-like Medium

In this chapter, the aim is to present the calculations needed to determine the dark matter-electron scattering rate in the solar medium. First, the relevant interaction Lagrangian will be presented before calculating the Feynman amplitude of the studied process. This can then be used to compute the cross section where the framework of linear response theory will play an important role in accounting for the in-medium effects. Finally, this cross section can be used to compute the relevant interaction rate. The chapter will conclude with a presentation of the behaviour of the interaction rate for different scenarios where the effect of the medium through linear response theory can be seen.

This chapter is based on the formalism presented in Ref. [45]. Similarly to how they proceeded there the scattering process that will be considered in this report has the Feynman diagram displayed in Figure 2.1. The idea is that the dark matter particle impinges on a fixed target consisting of the electrons in the Sun.

In the scattering process shown in Figure 2.1 the dark matter particle χ exchanges a four-momentum of $(\omega, \mathbf{Q})$ in the solar medium which takes the solar medium electrons from their initial energy eigenstate $|j\rangle$ to their final energy eigenstate $|i\rangle$. For the upcoming calculations $\omega > 0$ will correspond to the dark matter particle, χ, losing energy in the scattering event and $\omega < 0$ will correspond to the dark matter particle, χ, gaining energy in the scattering event.

2.1 The Interaction Lagrangian

Consider a Dirac type particle, χ, coupling to the electrons, e, via a heavy dark photon, A'_μ, the relevant interaction Lagrangian is given by

$$\mathcal{L}_{\text{int}} = g_\chi \bar{\chi} \gamma^\mu \chi A'_\mu + g_e \bar{e} \gamma^\mu e A'_\mu \tag{2.1}$$

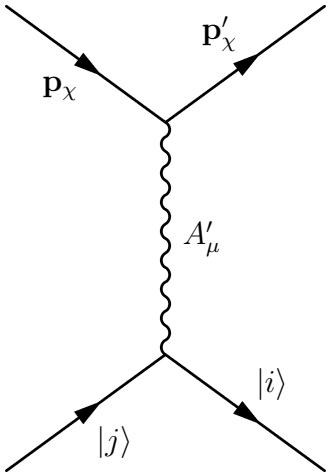

Figure 2.1: The Feynman diagram for the studied process with a dark matter Dirac fermion χ that interacts with the electrons of the solar medium via a massive dark photon mediator A'_μ.

where g_χ and g_e are the coupling constants between the dark photon A'_μ and the dark matter particle χ and the electrons, e, respectively. This Lagrangian is the full relativistic Lagrangian for the process, however, in this report, only the non-relativistic part is of interest. This should be a reasonable assumption since neither the typical dark matter velocities nor the typical velocities of the electrons in the Sun reach relativistic speeds. This means that it will be enough to consider the non-relativistic effective field theory Lagrangian to leading order where the interactions reduce to

$$\mathcal{L}_{\text{int}}^{\text{eff}} = g_e A'_0 \psi_e^\dagger \psi_e + g_\chi A'_0 \psi_\chi^\dagger \psi_\chi \tag{2.2}$$

similarly, the interactions between electron-electron and electron-ion via a standard model photon are reduced to

$$\mathcal{L}_{Ae}^{\text{eff}} \supset -(Z) e A_0 \psi_e^\dagger \psi_e, \tag{2.3}$$

where ψ_e and ψ_χ are the non-relativistic wave functions for the electron and dark matter particle respectively, e is the QED coupling constant and Z is the charge number of the ion. In these effective field theory Lagrangians one important feature is that they only depend on the zeroth component of the mediators (A_μ and A'_μ respectively) meaning that the vector mediators here reduce to scalar mediators.

To take the step from the relativistic interaction Lagrangian to these effective Lagrangians one can follow the procedure of Ref. [53]. There they start by looking at how the electrons couple to the photons in the standard model via electromagnetism through the Lagrangian

$$\mathcal{L}_e = \bar{e}(\mathbf{x}, t)(i\gamma^\mu(\partial_\mu + ie\mathcal{A}_\mu) - m_e)e(\mathbf{x}, t) \tag{2.4}$$

where it is worth noting that the interaction term $\bar{e}(\mathbf{x}, t)\gamma^\mu e\mathcal{A}_\mu e(\mathbf{x}, t)$ is analogous to the terms in Equation (2.1). By now writing the relativistic electron field, $e(\mathbf{x}, t)$, as

$$e(\mathbf{x}, t) = e^{-im_e t}\psi_e(\mathbf{x}, t) \tag{2.5}$$

the Lagrangian in Equation (2.4) becomes

$$\begin{aligned}\mathcal{L}_e = \psi_e^\dagger e^{im_e t}\gamma^0(i\gamma^0(\partial_t + ie\mathcal{A}_0) + i\boldsymbol{\gamma}\cdot(\nabla - ie\mathcal{A}) - m_e)e^{-im_e t}\psi_e = \\ \psi_e^\dagger(i\partial_t - e\mathcal{A}_0 - i\gamma^0\boldsymbol{\gamma}\cdot(\nabla - ie\mathcal{A}) - (1-\gamma^0)m_e)\psi_e.\end{aligned} \tag{2.6}$$

Defining the projection operator as $P_\pm \equiv \frac{1}{2}(1 \pm \gamma^0)$ and $\psi_e^\pm \equiv P_\pm\psi_e$ the Lagrangian can be rewritten into

$$\begin{aligned}\mathcal{L}_e = \psi_e^{+\dagger}(i\partial_t - e\mathcal{A}_0)\psi_e^+ + \psi_e^{-\dagger}(i\partial_t - e\mathcal{A}_0 + 2m_e)\psi_e^- + \\ \psi_e^{+\dagger}i\boldsymbol{\gamma}\cdot(\nabla - ie\mathcal{A})\psi_e^- - \psi_e^{-\dagger}i\boldsymbol{\gamma}\cdot(\nabla - ie\mathcal{A})\psi_e^+.\end{aligned} \tag{2.7}$$

Using the Equation of motion for the massive ψ_e^- field it can be written

$$\psi_e^- = \frac{1}{2m_e + i\partial_t - e\mathcal{A}_0} i\boldsymbol{\gamma}\cdot(\nabla - ie\mathcal{A})\psi_e^+ \tag{2.8}$$

and thus the Lagrangian arrives at its EFT form given by

$$\mathcal{L}_e^{\text{eff}} = \psi_e^{+\dagger}(i\partial_t - e\mathcal{A}_0 + ...)\psi_e^+ \tag{2.9}$$

where the ... part of the expression contains all terms with a higher order of e or factors $\frac{\nabla}{m_e}$ which are subject to velocity suppression and thus also ignored in this work [45]. Using $\mathcal{A}_0 = \phi + A_0$ where ϕ is the electrostatic background and A_0 is from the photon quanta, A_μ, the effective interaction becomes the expression in Equation (2.3) and a similar derivation leads to the effective interactions in Equation (2.2).

2.2 Feynman Amplitude

To calculate the cross section of the process in Figure 2.1 the corresponding S-matrix element needs to be calculated. For this calculation the expansions of ψ_χ and $\psi_\chi^\dagger$ are needed and those are given by

$$\psi_\chi = \int \frac{d^3\mathbf{p}}{(2\pi)^3}\sum_s \hat{a}_{s\mathbf{p}}e^{-ip\cdot x}\begin{pmatrix}\xi_s \\ \xi_s\end{pmatrix} \tag{2.10}$$

$$\psi_\chi^\dagger = \int \frac{d^3\mathbf{p}}{(2\pi)^3}\sum_s \hat{a}_{s\mathbf{p}}^\dagger e^{ip\cdot x}\begin{pmatrix}\xi_s^\dagger \\ \xi_s^\dagger\end{pmatrix}^\dagger \tag{2.11}$$

where $\xi_+ = \frac{1}{\sqrt{2}}\begin{pmatrix}1\\0\end{pmatrix}$, $\xi_- = \frac{1}{\sqrt{2}}\begin{pmatrix}0\\1\end{pmatrix}$ and the creation and annihilation operators follow the anticommutation relation $\{\hat{a}_{s\mathbf{p}}, \hat{a}_{s\mathbf{p}}^\dagger\} = (2\pi)^3\delta^{(3)}(\mathbf{p}-\mathbf{p}')\delta_{s,s'}$ [53]. The S-matrix element for the interaction in Figure 2.1, using the Lagrangian in Equation (2.2), is given by

$$S_{fi}^{(2)} = -\int d^4x_1 \int d^4x_2 \langle p'_\chi, i|(g_\chi\overbrace{\psi_\chi^\dagger\psi_\chi}A'_{0})_{x_1}(g_e\overbrace{A'_0\psi_e^\dagger\psi_e}|_{x_2}|p_\chi, j\rangle \tag{2.12}$$

where

$$\overbrace{A'_0 A'_0} = \int \frac{d^4Q}{(2\pi)^4} \frac{i}{Q^2 - m_{A'}^2} e^{iQ\cdot(x_1 - x_2)} \tag{2.13}$$

$$\langle \overbrace{p'_\chi | \psi^\dagger_\chi} = \langle 0 | \, e^{ip'_\chi \cdot x_1} \begin{pmatrix} \xi^\dagger_{s'} \\ \xi^\dagger_{s'} \end{pmatrix}^\dagger \tag{2.14}$$

$$\overbrace{\psi_\chi | p_\chi \rangle} = \begin{pmatrix} \xi_s \\ \xi_s \end{pmatrix} e^{-ip_\chi \cdot x_1} \, |0\rangle \tag{2.15}$$

$$\langle i | \, \psi^\dagger_e(t_2, \mathbf{x}_2) \psi_e(t_2, \mathbf{x}_2) \, | j \rangle = \langle i | \, e^{i\varepsilon_i t_2} \psi^\dagger_e(\mathbf{x}_2) e^{-i\varepsilon_j t_2} \psi_e(\mathbf{x}_2) \, | j \rangle \tag{2.16}$$

and where $m_{A'}$ is the mass of the mediator and ε_j and ε_i are the initial and final energy of the electrons. Using these equalities the expression in Equation (2.12) can be rewritten according to

$$\begin{aligned} S^{(2)}_{fi} = -ig_e g_\chi \int d^4x_1 \int d^3\mathbf{x}_2 \int dt_2 \, \langle i | \int \frac{dQ^4}{(2\pi)^4} \frac{1}{Q^2 - m_{A'}^2} e^{iQ\cdot x_1} e^{-iQ\cdot x_2} \\ e^{ip'_\chi \cdot x_1} e^{-ip_\chi \cdot x_1} e^{-\varepsilon_j t_2} e^{i\varepsilon_i t_2} \psi^\dagger_e \psi_e \, | j \rangle \begin{pmatrix} \xi^\dagger_{s'} \\ \xi^\dagger_{s'} \end{pmatrix}^\dagger \begin{pmatrix} \xi_s \\ \xi_s \end{pmatrix}. \end{aligned} \tag{2.17}$$

To simplify the expression for $S^{(2)}_{fi}$ further the relations

$$\int d^4x_1 e^{iQ\cdot x_1} e^{ip'_\chi \cdot x_1} e^{-ip_\chi \cdot x_1} = (2\pi)^4 \delta^{(4)}(Q + p'_\chi - p_\chi) \tag{2.18}$$

$$\int dt_2 e^{-it_2\omega} e^{\mathbf{Q}\cdot\mathbf{x}_2} e^{-i\varepsilon_j t_2} e^{i\varepsilon_i t_2} = e^{\mathbf{Q}\cdot\mathbf{x}_2} (2\pi) \delta(\omega - \varepsilon_i + \varepsilon_j) \tag{2.19}$$

can be used, leading to

$$\begin{aligned} S^{(2)}_{fi} = -ig_e g_\chi \int d^3\mathbf{x}_2 \int d^4Q \frac{1}{Q^2 - m_{A'}^2} \, \langle i | \, e^{\mathbf{Q}\cdot\mathbf{x}_2} \psi^\dagger_e \psi_e \, | j \rangle \\ \delta^{(4)}(Q + p'_\chi - p_\chi) 2\pi \delta(\omega - \varepsilon_i + \varepsilon_j) \begin{pmatrix} \xi^\dagger_{s'} \\ \xi^\dagger_{s'} \end{pmatrix}^\dagger \begin{pmatrix} \xi_s \\ \xi_s \end{pmatrix}. \end{aligned} \tag{2.20}$$

By defining

$$\psi^\dagger_e \psi_e \equiv \rho_e \tag{2.21}$$

$$\frac{p'^2_\chi}{2m_\chi} - \frac{p^2_\chi}{2m_\chi} \equiv \omega_{p'p} \tag{2.22}$$

where $\omega_{p'p}$ is the energy gain of the dark matter particle and ρ_e is the density operator and also renaming $\mathbf{x}_2$ into $\mathbf{x}$ the expression for $S^{(2)}_{fi}$ can be written as

$$\begin{aligned} S^{(2)}_{fi} = \int d^3\mathbf{x} \int d^4Q \frac{-ig_e g_\chi}{\omega^2 - \mathbf{Q}^2 - m_{A'}^2} \, \langle i | \, e^{\mathbf{Q}\cdot\mathbf{x}_2} \rho_e \, | j \rangle \\ \delta^{(3)}(\mathbf{Q} + \mathbf{p}'_\chi - \mathbf{p}_\chi) 2\pi \delta(\omega_{p'p} + \omega) \delta(\omega - \varepsilon_i + \varepsilon_j) \begin{pmatrix} \xi^\dagger_{s'} \\ \xi^\dagger_{s'} \end{pmatrix}^\dagger \begin{pmatrix} \xi_s \\ \xi_s \end{pmatrix}. \end{aligned} \tag{2.23}$$

Due to the process being in the non-relativistic limit $\omega^2 - \mathbf{Q}^2 - m_{A'}^2 \approx -(\mathbf{Q}^2 + m_{A'}^2)$ and therefore

$$\begin{aligned} S_{fi}^{(2)} \approx \int d^3\mathbf{x} \int d^4Q \frac{ig_e g_\chi}{\mathbf{Q}^2 + m_{A'}^2} \langle i| e^{\mathbf{Q}\cdot\mathbf{x}} \rho_e |j\rangle \\ \delta^{(3)}(\mathbf{Q} + \mathbf{p}'_\chi - \mathbf{p}_\chi) 2\pi\delta(\omega_{p'p} + \omega)\delta(\omega - \varepsilon_i + \varepsilon_j) \begin{pmatrix} \xi^\dagger_{s'} \\ \xi^\dagger_{s'} \end{pmatrix}^\dagger \begin{pmatrix} \xi_s \\ \xi_s \end{pmatrix}. \end{aligned} \tag{2.24}$$

If Q is redefined as $|\mathbf{Q}| = Q$ the expression for $S_{fi}^{(2)}$ becomes

$$\begin{aligned} S_{fi}^{(2)} \approx \int d\omega\delta(\omega - \varepsilon_i + \varepsilon_j) \int d^3\mathbf{Q}\delta^{(3)}(\mathbf{Q} + \mathbf{p}'_\chi - \mathbf{p}_\chi) \frac{ig_e g_\chi}{Q^2 + m_{A'}^2} \\ \int_V d^3\mathbf{x} \langle i| e^{\mathbf{Q}\cdot\mathbf{x}} \rho_e |j\rangle 2\pi\delta(\omega_{p'p} + \omega) \begin{pmatrix} \xi^\dagger_{s'} \\ \xi^\dagger_{s'} \end{pmatrix}^\dagger \begin{pmatrix} \xi_s \\ \xi_s \end{pmatrix} \end{aligned} \tag{2.25}$$

where, in particular, the Feynman amplitude $i\mathcal{M}_{j\to i}$ can be identified as

$$\begin{aligned} i\mathcal{M}_{j\to i} = \int d\omega\delta(\omega - \varepsilon_i + \varepsilon_j) \int d^3\mathbf{Q}\delta^{(3)}(\mathbf{Q} + \mathbf{p}'_\chi - \mathbf{p}_\chi) \\ \frac{ig_e g_\chi}{Q^2 + m_{A'}^2} \int_V d^3\mathbf{x} \langle i| e^{\mathbf{Q}\cdot\mathbf{x}} \rho_e |j\rangle \begin{pmatrix} \xi^\dagger_{s'} \\ \xi^\dagger_{s'} \end{pmatrix}^\dagger \begin{pmatrix} \xi_s \\ \xi_s \end{pmatrix}. \end{aligned} \tag{2.26}$$

2.3 Cross Section

Using the expression presented in Ref. [45] for the effective cross section for the excitation channel $j \to i$ it can be written as

$$\sigma_{j\to i} = \int \frac{d^3p'_\chi}{(2\pi)^3} \frac{|\mathcal{M}_{j\to i}|^2}{v_\chi} 2\pi\delta(\omega_{p'p} + \varepsilon_i - \varepsilon_j) \tag{2.27}$$

where v_χ is the velocity of the incoming dark matter particle. Using the above calculated matrix element, and averaging and summing over all the initial and final states, respectively, the total cross section can be expressed as

$$\begin{aligned} \sigma(v_\chi) = \sum_{ij} \int d\omega\delta(\omega - \varepsilon_i + \varepsilon_j) \int d^3\mathbf{Q}\delta^{(3)}(\mathbf{Q} + \mathbf{p}'_\chi - \mathbf{p}_\chi) \int \frac{d^3p'_\chi}{(2\pi)^3} \frac{1}{v_\chi} \\ \Big(\frac{g_e g_\chi}{Q^2 + m_{A'}^2}\Big)^2 \int_V d^3\mathbf{x} d^3\mathbf{x}' p_j \langle j| e^{-\mathbf{Q}\cdot\mathbf{x}} \rho_e(\mathbf{x}) |i\rangle \langle i| e^{\mathbf{Q}\cdot\mathbf{x}'} \rho_e(\mathbf{x}') |j\rangle 2\pi\delta(\omega_{p'p} + \omega) \end{aligned} \tag{2.28}$$

where p_j is the thermal distribution of the initial electron state $|j\rangle$. Note that the summing and averaging over the initial and final states of the dark matter sums up to one due to

$$\frac{1}{2}\sum_{ss'} \begin{pmatrix} \xi^\dagger_{s'} \\ \xi^\dagger_{s'} \end{pmatrix}^\dagger \begin{pmatrix} \xi_s \\ \xi_s \end{pmatrix} \begin{pmatrix} \xi^\dagger_s \\ \xi^\dagger_s \end{pmatrix}^\dagger \begin{pmatrix} \xi_{s'} \\ \xi_{s'} \end{pmatrix} = \frac{1}{2}\sum_{s'} \begin{pmatrix} \xi^\dagger_{s'} \\ \xi^\dagger_{s'} \end{pmatrix}^\dagger \left(\sum_s \begin{pmatrix} \xi_s \\ \xi_s \end{pmatrix} \begin{pmatrix} \xi^\dagger_s \\ \xi^\dagger_s \end{pmatrix}^\dagger \right) \begin{pmatrix} \xi_{s'} \\ \xi_{s'} \end{pmatrix} \tag{2.29}$$

where

$$\sum_s \begin{pmatrix}\xi_s\\ \xi_s\end{pmatrix}\begin{pmatrix}\xi_s^\dagger\\ \xi_s^\dagger\end{pmatrix}^\dagger = \frac{1}{2}\left(\begin{pmatrix}1\\0\\1\\0\end{pmatrix}\begin{pmatrix}1 & 0 & 1 & 0\end{pmatrix} + \begin{pmatrix}0\\1\\0\\1\end{pmatrix}\begin{pmatrix}0 & 1 & 0 & 1\end{pmatrix}\right) = \frac{1}{2}\begin{pmatrix}1&0&1&0\\0&1&0&1\\1&0&1&0\\0&1&0&1\end{pmatrix} \tag{2.30}$$

leading to

$$\begin{aligned}\frac{1}{2}\sum_{s'}\begin{pmatrix}\xi_{s'}^\dagger\\ \xi_{s'}^\dagger\end{pmatrix}^\dagger\left(\sum_s\begin{pmatrix}\xi_s\\ \xi_s\end{pmatrix}\begin{pmatrix}\xi_s^\dagger\\ \xi_s^\dagger\end{pmatrix}^\dagger\right)\begin{pmatrix}\xi_{s'}\\ \xi_{s'}\end{pmatrix} = \frac{1}{8}\Bigg(&\begin{pmatrix}1 & 0 & 1 & 0\end{pmatrix}\begin{pmatrix}1&0&1&0\\0&1&0&1\\1&0&1&0\\0&1&0&1\end{pmatrix}\begin{pmatrix}1\\0\\1\\0\end{pmatrix}\\ &+\begin{pmatrix}0 & 1 & 0 & 1\end{pmatrix}\begin{pmatrix}1&0&1&0\\0&1&0&1\\1&0&1&0\\0&1&0&1\end{pmatrix}\begin{pmatrix}0\\1\\0\\1\end{pmatrix}\Bigg) = \frac{1}{8}(4+4) = 1.\end{aligned} \tag{2.31}$$

Now, by using the fact that

$$2\pi\delta(\omega-\varepsilon_i+\varepsilon_j) = \int_{-\infty}^{\infty} dt e^{i\omega(t-0)}e^{i\varepsilon_j t - i\varepsilon_i t} \tag{2.32}$$

a part of the expression for the cross section can be rewritten according to

$$\begin{aligned}\sum_{ij} 2\pi\delta(\omega-\varepsilon_i+\varepsilon_j)p_j\left\langle j\right|\rho_e(\mathbf{x})\left|i\right\rangle\left\langle i\right|\rho_e(\mathbf{x}')\left|j\right\rangle &=\\ \sum_{ij}\int_{-\infty}^{\infty} dt p_j\left\langle j\right|\rho_e(\mathbf{x})\left|i\right\rangle\left\langle i\right|\rho_e(\mathbf{x}')\left|j\right\rangle e^{i\omega(t-0)}e^{i\varepsilon_j t-i\varepsilon_i t} &=\\ \sum_{ij}\int_{-\infty}^{\infty} dt p_j\left\langle j\right|e^{iH_0 t}\rho_e(\mathbf{x})e^{-iH_0 t}\left|i\right\rangle\left\langle i\right|e^{iH_0 0}\rho_e(\mathbf{x}')e^{-iH_0 0}\left|j\right\rangle e^{i\omega(t-0)} &=\\ \int_{-\infty}^{\infty} dt\langle\rho_{eI}(\mathbf{x},t)\rho_{eI}(\mathbf{x}',0)\rangle e^{i\omega(t-0)}&\end{aligned} \tag{2.33}$$

where H_0 is the Hamiltonian of the unperturbed system of which $|i\rangle$ and $|j\rangle$ are eigenstates, $\rho_{eI}(\mathbf{x},t) = e^{iH_0t}\rho_e(\mathbf{x})e^{-iH_0t}$ is the density operator in the interaction picture and the part containing $\langle ...\rangle$ denotes the thermal average. By also utilising that

$$\int d^3p'_\chi\delta^{(3)}(\mathbf{Q}+\mathbf{p}'_\chi-\mathbf{p}_\chi) \tag{2.34}$$

sets $\mathbf{p}'_\chi = \mathbf{p}_\chi - \mathbf{Q}$ the expression for $\omega_{p'p}$ can be rewritten into

$$\omega_{p'p} = \frac{p'^2_\chi}{2m_\chi} - \frac{p^2_\chi}{2m_\chi} = \frac{p^2_\chi}{2m_\chi} - \frac{2\mathbf{p}_\chi\cdot\mathbf{Q}}{2m_\chi} + \frac{Q^2}{2m_\chi} - \frac{p^2_\chi}{2m_\chi} = \frac{Q^2}{2m_\chi} - \mathbf{v}_\chi\cdot\mathbf{Q} \tag{2.35}$$

where the relation $\frac{\mathbf{p}_\chi}{m_\chi} = \mathbf{v}_\chi$ were used. This leads to

$$\begin{aligned}\sigma(v_\chi) = \int d\omega\int\frac{d^3Q}{(2\pi)^3}\frac{1}{v_\chi}\Big(\frac{g_e g_\chi}{Q^2+m^2_{A'}}\Big)^2\int_V d^3\mathbf{x}d^3\mathbf{x}'&\\ \int_{-\infty}^{\infty} dt\langle\rho_{eI}(\mathbf{x},t)\rho_{eI}(\mathbf{x}',0)\rangle e^{i\omega(t-0)}e^{\mathbf{Q}\cdot(\mathbf{x}'-\mathbf{x})}\delta(\frac{Q^2}{2m_\chi}-\mathbf{v}_\chi\cdot\mathbf{Q}+\omega)&\end{aligned} \tag{2.36}$$

where the dynamical structure factor, presented in Appendix B, can be utilised. The dynamical structure factor, $S(\omega, \mathbf{Q})$, is defined as

$$S(\omega, \mathbf{Q}) \equiv \frac{1}{V} \int_V d^3\mathbf{x} d^3\mathbf{x}' \int_{-\infty}^{\infty} dt \langle \rho_{eI}(\mathbf{x}, t) \rho_{eI}(\mathbf{x}', 0) \rangle e^{i\omega(t-0)} e^{\mathbf{Q}\cdot(\mathbf{x}'-\mathbf{x})}. \tag{2.37}$$

By using the fluctuation-dissipation theorem, presented in Appendix A, that states

$$S(\omega, \mathbf{Q}) = -2 \frac{1}{1 - e^{-\beta\omega}} \mathrm{Im}(\chi_{\rho\rho}(\omega, \mathbf{Q})) \tag{2.38}$$

where $\chi_{\rho\rho}(\omega, \mathbf{Q})$ is the density-density response function introduced in Appendix B, Equation (2.36) can be rewritten as

$$\sigma(v_\chi) = V \int d\omega \int \frac{d^3Q}{(2\pi)^3} \frac{1}{v_\chi} \Big(\frac{g_e g_\chi}{Q^2 + m_{A'}^2} \Big)^2 \frac{(-2)\mathrm{Im}(\chi_{\rho\rho}(\omega, \mathbf{Q}))}{1 - e^{-\beta\omega}} \delta\Big(\frac{Q^2}{2m_\chi} - \mathbf{v}_\chi \cdot \mathbf{Q} + \omega \Big). \tag{2.39}$$

Introducing the reference cross section for the dark matter-electron interaction

$$\bar{\sigma_e} = \frac{\mu_{\chi e}^2}{\pi} \Big(\frac{g_\chi g_e}{\alpha m_e^2 + m_{A'}^2} \Big)^2 \tag{2.40}$$

where m_e is the mass of the electron, and $\mu_{\chi e}$ is the reduced mass of the electron and the dark matter particle, the expression for the total cross section, $\sigma(v_\chi)$, becomes

$$\sigma(v_\chi) = V \int d\omega \int \frac{d^3Q}{(2\pi)^3} \frac{\pi \bar{\sigma_e}}{v_\chi \mu_{\chi e}^2} \Big(\frac{\alpha m_e^2 + m_{A'}^2}{Q^2 + m_{A'}^2} \Big)^2 \frac{(-2)\mathrm{Im}(\chi_{\rho\rho}(\omega, \mathbf{Q}))}{1 - e^{-\beta\omega}} \delta\Big(\frac{Q^2}{2m_\chi} - \mathbf{v}_\chi \cdot \mathbf{Q} + \omega \Big). \tag{2.41}$$

Note that, in Equation (2.41), the factor $\Big(\frac{\alpha m_e^2 + m_{A'}^2}{Q^2 + m_{A'}^2} \Big)$ reduces to 1 and $\frac{\alpha m_e^2}{Q^2}$ in the heavy ($m_{A'}^2 \gg Q^2$, αm_e^2) and the light ($m_{A'}^2 \ll Q^2$, αm_e^2) mediator limit respectively.

Now would be a good time to take a step back to look at the expression for the cross section in Equation (2.41). One of the most important features in this expression is the density-density response function $\chi_{\rho\rho}$ since that is where the in-medium effect takes place. Therefore, in the coming section, we will take a closer look at this density-density response function, calculating it in a solar-like medium.

2.4 Density-Density Response Function in Solar-like Medium

This section will present the aspects of linear response theory that are most important for this thesis, primarily the density-density response function $\chi_{\rho\rho}(\omega, \mathbf{Q})$ in a solar-like medium. A more thorough introduction to the field of linear response theory can be found in Appendix A.

The density-density response function, $\chi_{\rho\rho}(\omega, \mathbf{Q})$, is given by

$\chi_{\rho\rho}(\omega, \mathbf{Q}) =$ 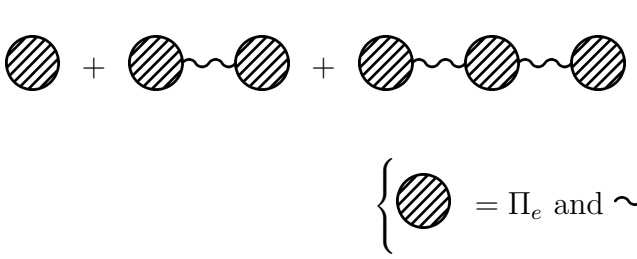 $+ \ldots =$ 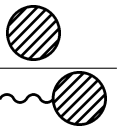 $=$

$$\left\{ \text{} = \Pi_e \text{ and } \text{} = V_e \right\} = \frac{\Pi_e}{1 - V_e \Pi_e} \tag{2.42}$$

where the wavy line, denoted V_e, is the coulomb interaction given by $V_e = \frac{e^2}{Q^2}$ and the one-particle-irreducible (1PI), denoted Π_e, can be approximated as the electron pair bubble in the random phase approximation (RPA)

$$\Pi_e = \frac{1}{V} \sum_{\mathbf{p}} \frac{f_{\mathbf{p}} - f_{\mathbf{p}+\mathbf{Q}}}{\omega - (\varepsilon_{\mathbf{p}+\mathbf{Q}} - \varepsilon_{\mathbf{p}}) + i0^+} \tag{2.43}$$

where $f_{\mathbf{p}}$ denote the occupation number and $\varepsilon_{\mathbf{p}} = \frac{p^2}{2m_e}$ is the energy of a free electron with momentum $\mathbf{p}$, assuming non relativistic energies [45]. If the relation $n_e \left(\frac{2\pi}{m_e T}\right)^{3/2} \ll 1$, where n_e is the electron number density and T is the temperature, is fulfilled, which it is in the Sun, the occupation number, $f_{\mathbf{p}}$, can be described with Boltzmann form

$$f_{\mathbf{p}} = n_e \left(\sqrt{\frac{2\pi}{m_e T}}\right)^3 \exp\left(-\frac{p^2}{2m_e T}\right). \tag{2.44}$$

Using the fact that the sum in Equation (2.43) goes over all $\mathbf{p}$ it can be rewritten

$$\begin{aligned} &\frac{1}{V} \sum_{\mathbf{p}} \frac{f_{\mathbf{p}} - f_{\mathbf{p}+\mathbf{Q}}}{\omega - (\varepsilon_{\mathbf{p}+\mathbf{Q}} - \varepsilon_{\mathbf{p}}) + i0^+} = \\ &\frac{1}{V} \left(\sum_{\mathbf{p}} \frac{f_{\mathbf{p}}}{\omega - (\varepsilon_{\mathbf{p}+\mathbf{Q}} - \varepsilon_{\mathbf{p}}) + i0^+} - \sum_{\mathbf{p}} \frac{f_{\mathbf{p}+\mathbf{Q}}}{\omega - (\varepsilon_{\mathbf{p}+\mathbf{Q}} - \varepsilon_{\mathbf{p}}) + i0^+} \right) = \\ &\frac{1}{V} \left(\sum_{\mathbf{p}} \frac{f_{-\mathbf{p}-\frac{\mathbf{Q}}{2}}}{\omega - (\varepsilon_{-\mathbf{p}+\frac{\mathbf{Q}}{2}} - \varepsilon_{-\mathbf{p}-\frac{\mathbf{Q}}{2}}) + i0^+} - \sum_{\mathbf{p}} \frac{f_{\mathbf{p}+\frac{\mathbf{Q}}{2}}}{\omega - (\varepsilon_{\mathbf{p}+\frac{\mathbf{Q}}{2}} - \varepsilon_{\mathbf{p}-\frac{\mathbf{Q}}{2}}) + i0^+} \right) \end{aligned} \tag{2.45}$$

and by using

$$\varepsilon_{-\mathbf{p}+\frac{\mathbf{Q}}{2}} - \varepsilon_{-\mathbf{p}-\frac{\mathbf{Q}}{2}} = \frac{1}{2m_e} \left(p^2 - \mathbf{p} \cdot \mathbf{Q} + \frac{Q^2}{4} - p^2 - \mathbf{p} \cdot \mathbf{Q} - \frac{Q^2}{4} \right) = -\frac{\mathbf{p} \cdot \mathbf{Q}}{m_e} \tag{2.46}$$

$$\varepsilon_{\mathbf{p}+\frac{\mathbf{Q}}{2}} - \varepsilon_{\mathbf{p}-\frac{\mathbf{Q}}{2}} = \frac{1}{2m_e} \left(p^2 + \mathbf{p} \cdot \mathbf{Q} + \frac{Q^2}{4} - p^2 + \mathbf{p} \cdot \mathbf{Q} - \frac{Q^2}{4} \right) = \frac{\mathbf{p} \cdot \mathbf{Q}}{m_e} \tag{2.47}$$

and the fact that $f_{-\mathbf{p}} = f_{\mathbf{p}}$ the expression in Equation (2.43) becomes

$$\Pi_e = \frac{1}{V} \sum_{\mathbf{p}} f_{\mathbf{p}+\frac{\mathbf{Q}}{2}} \left(\frac{1}{\omega + \frac{\mathbf{p} \cdot \mathbf{Q}}{m_e} + i0^+} - \frac{1}{\omega - \frac{\mathbf{p} \cdot \mathbf{Q}}{m_e} + i0^+} \right). \tag{2.48}$$

The sum $\sum_{\mathbf{p}} \sim \frac{V}{(2\pi)^3}\int d^3p$ and therefore

$$\begin{aligned}\Pi_e = \int \frac{d^3p}{(2\pi)^3} f_{\mathbf{p}+\frac{\mathbf{Q}}{\mathbf{2}}}\left(\frac{1}{\omega+\frac{\mathbf{p}\cdot\mathbf{Q}}{m_e}+i0^+}-\frac{1}{\omega-\frac{\mathbf{p}\cdot\mathbf{Q}}{m_e}+i0^+}\right) = \\ n_e\left(\sqrt{\frac{2\pi}{m_eT}}\right)^3\int\frac{d^3p}{(2\pi)^3}\exp\left(-\frac{|\mathbf{p}+\frac{\mathbf{Q}}{\mathbf{2}}|^2}{2m_eT}\right)(...)\end{aligned} \tag{2.49}$$

where the factor (...) in the second line contains the terms in the parenthesis in the first line. Splitting up $\mathbf{p}$ in one component parallel and one component perpendicular to $\mathbf{Q}$ leads to

$$\begin{aligned}\Pi_e = n_e\left(\sqrt{\frac{2\pi}{m_eT}}\right)^3\int\frac{d^2p_\perp}{(2\pi)^2}\exp\left(-\frac{p_\perp^2}{2m_eT}\right)\int_{-\infty}^{\infty}\frac{dp_\parallel}{2\pi}\exp\left(-\frac{(p_\parallel+\frac{Q}{2})^2}{2m_eT}\right)(...) = \\ n_e\sqrt{\frac{2\pi}{m_eT}}\int_{-\infty}^{\infty}\frac{dp_\parallel}{2\pi}\exp\left(-\frac{(p_\parallel+\frac{Q}{2})^2}{2m_eT}\right)\left(\frac{1}{\omega+\frac{p_\parallel Q}{m_e}+i0^+}-\frac{1}{\omega-\frac{p_\parallel Q}{m_e}+i0^+}\right).\end{aligned} \tag{2.50}$$

Using the mathematical relation

$$\frac{1}{x\pm i0^+} = \mathcal{P}\frac{1}{x}\mp i\pi\delta(x), \tag{2.51}$$

where $\mathcal{P}$ is the so-called Cauchy principal value, the expression for Π_e can be written

$$\begin{aligned}\Pi_e = n_e\sqrt{\frac{2\pi}{m_eT}}\mathcal{P}\int_{-\infty}^{\infty}\frac{dp_\parallel}{2\pi}\exp\left(-\frac{(p_\parallel+\frac{Q}{2})^2}{2m_eT}\right)\left(\frac{1}{\omega+\frac{p_\parallel Q}{m_e}}-\frac{1}{\omega-\frac{p_\parallel Q}{m_e}}\right) \\ -i\pi n_e\sqrt{\frac{2\pi}{m_eT}}\int_{-\infty}^{\infty}\frac{dp_\parallel}{2\pi}\exp\left(-\frac{(p_\parallel+\frac{Q}{2})^2}{2m_eT}\right)\left(\delta\left(\omega+\frac{p_\parallel Q}{m_e}\right)-\delta\left(\omega-\frac{p_\parallel Q}{m_e}\right)\right).\end{aligned} \tag{2.52}$$

Rewriting the imaginary part of Π_e yields

$$\begin{aligned}\mathrm{Im}(\Pi_e) = -\pi n_e\sqrt{\frac{2\pi}{m_eT}}\int_{-\infty}^{\infty}\frac{dp_\parallel}{2\pi}\exp\left(-\frac{(p_\parallel+\frac{Q}{2})^2}{2m_eT}\right)\left(\delta\left(\omega+\frac{p_\parallel Q}{m_e}\right)-\delta\left(\omega-\frac{p_\parallel Q}{m_e}\right)\right) = \\ -\pi n_e\sqrt{\frac{2\pi}{m_eT}}\frac{m_e}{Q}\int_{-\infty}^{\infty}\frac{dp_\parallel}{2\pi}\exp\left(-\frac{(p_\parallel+\frac{Q}{2})^2}{2m_eT}\right)\left(\delta\left(\frac{\omega m_e}{Q}+p_\parallel\right)-\delta\left(\frac{\omega m_e}{Q}-p_\parallel\right)\right) = \\ -\pi n_e\sqrt{\frac{2\pi}{m_eT}}\frac{m_e}{Q}\frac{1}{2\pi}\left(\exp\left(-\frac{(-\frac{\omega m_e}{Q}+\frac{Q}{2})^2}{2m_eT}\right)-\exp\left(-\frac{(\frac{\omega m_e}{Q}+\frac{Q}{2})^2}{2m_eT}\right)\right) = \\ -\pi n_e\sqrt{\frac{2\pi}{m_eT}}\frac{m_e}{Q}\frac{1}{2\pi}\left(\exp\left(-\frac{\frac{\omega^2m_e^2}{Q^2}-\omega m_e+\frac{Q^2}{4}}{2m_eT}\right)-\exp\left(-\frac{\frac{\omega^2m_e^2}{Q^2}+\omega m_e+\frac{Q^2}{4}}{2m_eT}\right)\right) = \\ -n_e\sqrt{\frac{2\pi}{m_eT}}\frac{m_e}{Q}\frac{1}{2}\exp\left(-\frac{\frac{\omega^2m_e^2}{Q^2}+\frac{Q^2}{4}}{2m_eT}\right)\left(\exp\left(\frac{\omega}{2T}\right)-\exp\left(-\frac{\omega}{2T}\right)\right) = \\ -n_e\sqrt{\frac{2\pi}{m_eT}}\frac{m_e}{Q}\exp\left(-\frac{\frac{\omega^2m_e^2}{Q^2}+\frac{Q^2}{4}}{2m_eT}\right)\sinh\left(\frac{\omega}{2T}\right).\end{aligned} \tag{2.53}$$

By now looking at the real part of Π_e using the substitution

$$y = \frac{p_\parallel + \frac{Q}{2}}{\sqrt{2m_eT}} \tag{2.54}$$

it can be rewritten according to

$$\begin{aligned}\mathrm{Re}(\Pi_e) = n_e\sqrt{\frac{2\pi}{m_eT}}\mathcal{P}\int_{-\infty}^{\infty}\frac{dp_\parallel}{2\pi}\exp\left(-\frac{(p_\parallel+\frac{Q}{2})^2}{2m_eT}\right)\left(\frac{1}{\omega+\frac{p_\parallel Q}{m_e}}-\frac{1}{\omega-\frac{p_\parallel Q}{m_e}}\right) = \\ \sqrt{2m_eT}n_e\sqrt{\frac{2\pi}{m_eT}}\mathcal{P}\int_{-\infty}^{\infty}\frac{dy}{2\pi}\exp\left(-y^2\right)\left(\frac{1}{\omega+\frac{\sqrt{2m_eT}Qy}{m_e}-\frac{Q^2}{2m_e}}-\frac{1}{\omega-\frac{\sqrt{2m_eT}Qy}{m_e}+\frac{Q^2}{2m_e}}\right) = \\ -n_e\frac{1}{Q}\sqrt{\frac{m_e}{2T}}\left(\phi\left(\sqrt{\frac{m_e}{2T}}\left(\frac{\omega}{Q}+\frac{Q}{2m_e}\right)\right)-\phi\left(\sqrt{\frac{m_e}{2T}}\left(\frac{\omega}{Q}-\frac{Q}{2m_e}\right)\right)\right)\end{aligned} \tag{2.55}$$

where ϕ is a function defined as

$$\phi(x) \equiv \mathcal{P}\int_{-\infty}^{\infty}\frac{dy}{\sqrt{\pi}}\frac{e^{-y^2}}{x-y}. \tag{2.56}$$

Using the rewritten variants of the real and imaginary part of Π_e, the full expression for Π_e become

$$\begin{aligned}\Pi_e(\omega,Q) = -n_e\frac{1}{Q}\sqrt{\frac{m_e}{2T}}\left(\phi\left(\sqrt{\frac{m_e}{2T}}\left(\frac{\omega}{Q}+\frac{Q}{2m_e}\right)\right)-\phi\left(\sqrt{\frac{m_e}{2T}}\left(\frac{\omega}{Q}-\frac{Q}{2m_e}\right)\right)\right) \\ -in_e\sqrt{\frac{2\pi}{m_eT}}\frac{m_e}{Q}\exp\left(-\frac{\frac{\omega^2m_e^2}{Q^2}+\frac{Q^2}{4}}{2m_eT}\right)\sinh\left(\frac{\omega}{2T}\right),\end{aligned} \tag{2.57}$$

notice in particular how Π_e is only a function of the magnitude of the transmitted momentum, Q, not $\mathbf{Q}$. Given the expression for the density-density response function $\chi_{\rho\rho}$ given in Equation (2.42) and how it is only dependent on V_e and Π_e, also the density-density response function is only a function of Q instead of $\mathbf{Q}$. The part of the density-density response function that will be especially interesting for us is its imaginary component. By using the so-called dielectric function, $\varepsilon(\omega, Q)$ presented in Appendix B, given by

$$\varepsilon(\omega,Q) = 1 - V_e\Pi_e \tag{2.58}$$

the imaginary part of the density-density response function can be expressed according to

$$\mathrm{Im}(\chi_{\rho\rho}) = \frac{\mathrm{Im}(\Pi_e)}{|\varepsilon|^2}. \tag{2.59}$$

In this way, all of the in-medium effects are packed into the dielectric function, ε, where $|\varepsilon|^2 > 1$ correspond to a screening effect and in contrast $|\varepsilon|^2 < 1$ correspond to a resonance caused by the medium.

For small energy and momentum transfers, specifically $\omega \ll 2T$ and $Q \ll \sqrt{2m_eT}$, the expression in Equation (2.57) can be rewritten using Taylor expansions. To do so, the derivative of the function $\phi(x)$, defined in Equation (2.56), is needed. By setting $\mathcal{P} = 1$, an expression for that can be calculated using integration by parts a couple of times

$$\begin{aligned}
\phi'(x) = -\frac{1}{\sqrt{\pi}}\int_{-\infty}^{\infty} dy \frac{e^{-y^2}}{(x-y)^2} = \\
-\frac{1}{\sqrt{\pi}}\left(\left[\frac{e^{-y^2}}{x-y}\right]_{-\infty}^{\infty} + \int_{-\infty}^{\infty}\frac{2y}{x-y}e^{-y^2}dy\right) = -\frac{2}{\sqrt{\pi}}\int_{-\infty}^{\infty}\frac{y}{x-y}e^{-y^2}dy = \\
-\frac{2}{\sqrt{\pi}}\left(\left[\frac{\sqrt{\pi}}{2}\mathrm{erf}(y)\frac{x}{x-y}\right]_{-\infty}^{\infty} - \frac{\sqrt{\pi}}{2}\int_{-\infty}^{\infty}\frac{x}{(x-y)^2}\mathrm{erf}(y)dy\right) = \\
2 + x\int_{-\infty}^{\infty}\frac{1}{(x-y)^2}\mathrm{erf}(y)dy = \\
2 + x\left[\frac{1}{x-y}\mathrm{erf}(y)\right]_{-\infty}^{\infty} - x\frac{2}{\sqrt{\pi}}\int_{-\infty}^{\infty}\frac{e^{-y^2}}{x-y}dy = 2 - 2x\phi(x).
\end{aligned} \tag{2.60}$$

Calling $a = \frac{Q}{2\sqrt{2m_eT}}$, which in the limit of $Q \ll \sqrt{2m_eT}$ is $\ll 1$, and $x = \sqrt{\frac{m_e}{2T}}\frac{\omega}{Q}$, the factor containing the ϕ functions in the real part of Equation (2.57) can be expressed as

$$\begin{aligned}
\phi(x+a) - \phi(x-a) \approx (\phi(x) + \phi'(x)a) - (\phi(x) - \phi'(x)a) = \\
2a\phi'(x) = 4a(1 - x\phi(x)) = \frac{4Q}{2\sqrt{2m_eT}}(1 - x\phi(x))
\end{aligned} \tag{2.61}$$

which leads to

$$\mathrm{Re}(\Pi_e) \approx -\frac{n_e}{Q}\sqrt{\frac{m_e}{2T}}\frac{4Q}{2\sqrt{2m_eT}}(1 - x\phi(x)) = -\frac{n_e}{T}(1 - x\phi(x)). \tag{2.62}$$

Also the imaginary part of Equation (2.57) can be simplified in these limits by utilising

$$\exp\left(-\frac{\frac{\omega^2 m_e^2}{Q^2} + \frac{Q^2}{4}}{2m_eT}\right) = \exp(-x^2)\exp(-\frac{Q^2}{8m_eT}) \approx \exp(-x^2) \tag{2.63}$$

$$\sinh\left(\frac{\omega}{2T}\right) \approx \frac{\omega}{2T}, \tag{2.64}$$

which, using $\frac{\omega}{2T} = x\frac{Q}{\sqrt{2m_eT}}$, leads to

$$\mathrm{Im}(\Pi_e) \approx -n_e\sqrt{\frac{2\pi}{m_eT}}\frac{m_e}{Q}\exp(-x^2)\frac{\omega}{2T} = -\sqrt{\pi}\frac{n_e}{T}x\exp(-x^2). \tag{2.65}$$

Therefore, in the limit of small energy and momentum transfer, Π_e is approximately

$$\Pi_e(\omega \to 0, Q \to 0) \approx -\frac{n_e}{T}(1 - x\phi(x)) - i\sqrt{\pi}\frac{n_e}{T}x\exp(-x^2). \tag{2.66}$$

2.4.1 Including Screening from the Ions in the Medium

So far the density-density response function has only taken into account the electrons of the medium. Directly, the dark matter particles only interact with the electrons in the model used in this thesis, but, since these electrons also can interact with the ions of the medium, the ions could induce further in-medium effects via indirect dark matter-ion interactions. Fortunately, the calculations needed to include the ions in the in-medium effects are, to a large extent, similar to those needed for the case demonstrated for only electrons. For the case where also ions are taken into account in the in-medium effect, the Equation for the density-density response function becomes

$\chi_{\rho\rho}(\omega, \mathbf{Q}) =$ 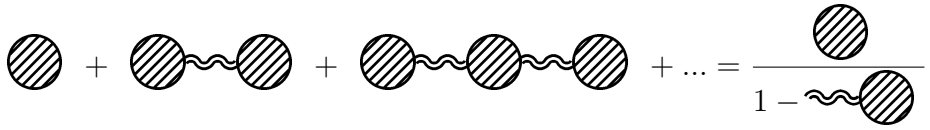 (2.67)

where the double wavy line is given by

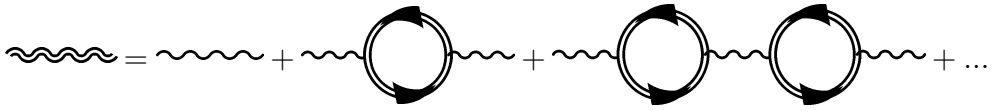

$$\begin{aligned} &= V_e + V_e(-Z)\Pi_N V_e(-Z) + V_e(-Z)\Pi_N V_e(-Z)^2\Pi_N V_e(-Z) + ... \\ &= \frac{V_e}{1 - V_e(-Z)^2\Pi_N}. \end{aligned} \tag{2.68}$$

Here Z is the charge number of the ion in question, and the loop, denoted Π_N, is the one particle irreducible at the RPA level of the ion [45]. In complete analogy to how Π_e were calculated Π_N can be obtained, leading to

$$\begin{aligned} \Pi_N = -n_N \frac{1}{Q}\sqrt{\frac{m_N}{2T}} \left(\phi\left(\sqrt{\frac{m_N}{2T}}\left(\frac{\omega}{Q} + \frac{Q}{2m_N}\right)\right) - \phi\left(\sqrt{\frac{m_N}{2T}}\left(\frac{\omega}{Q} - \frac{Q}{2m_N}\right)\right)\right) \\ -in_N\sqrt{\frac{2\pi}{m_N T}}\frac{m_N}{Q}\exp\left(-\frac{\frac{\omega^2 m_N^2}{Q^2} + \frac{Q^2}{4}}{2m_N T}\right)\sinh\left(\frac{\omega}{2T}\right) \end{aligned} \tag{2.69}$$

where n_N is the number density of the ion and m_N is the mass of the ion. Given this the expression for the density-density response function, $\chi_{\rho\rho}$, can be written according to

$$\chi_{\rho\rho} = \frac{\Pi_e}{1 - \frac{\Pi_e V_e}{1 - V_e\sum_i Z_i^2\Pi_{N_i}}} = \frac{\Pi_e(1 - V_e\sum_i Z_i^2\Pi_{N_i})}{1 - V_e\Pi_e - V_e\sum_i Z_i^2\Pi_{N_i}} \tag{2.70}$$

where the sum over i simply sums up the effect from all relevant ions. By expanding the expression for the density-density function, the imaginary part can be written as

$$\mathrm{Im}(\chi_{\rho\rho}) = \frac{|1 - V_e\sum_i Z_i^2\Pi_{N_i}|^2\mathrm{Im}(\Pi_e) + \sum_i |Z_i V_e\Pi_e|^2\mathrm{Im}(\Pi_{N_i})}{|1 - V_e\Pi_e - V_e\sum_i Z_i^2\Pi_{N_i}|^2}. \tag{2.71}$$

2.5 Scattering Rate

The scattering rate, Γ, between the dark matter particle and the solar medium electrons is given by

$$\Gamma(v_\chi) = \frac{v_\chi \sigma(\mathbf{v}_\chi)}{V} \tag{2.72}$$

where $\sigma(\mathbf{v}_\chi)$ were calculated in Section 2.3 and is given by the expression in Equation (2.41). Notice that, as pointed out in Section 2.4, the density-density response function, $\chi_{\rho\rho}$, is only a function of Q which makes it possible to rewrite the expression for the scattering rate

$$\begin{aligned}\Gamma(v_\chi) = \int d\omega \int \frac{d^3Q}{(2\pi)^3} \frac{\pi\bar{\sigma}_e}{\mu_{\chi e}^2} \Big(\frac{\alpha m_e^2 + m_{A'}^2}{Q^2 + m_{A'}^2}\Big)^2 \frac{(-2)\mathrm{Im}(\chi_{\rho\rho}(\omega, Q))}{1 - e^{-\beta\omega}} \delta(\frac{Q^2}{2m_\chi} - \mathbf{v}_\chi \cdot \mathbf{Q} + \omega) = \\ \int d\omega \int \frac{d^3Q}{(2\pi)^3} \frac{\pi\bar{\sigma}_e}{\mu_{\chi e}^2} \Big(\frac{\alpha m_e^2 + m_{A'}^2}{Q^2 + m_{A'}^2}\Big)^2 \frac{(-2)\mathrm{Im}(\chi_{\rho\rho}(\omega, Q))}{1 - e^{-\beta\omega}} \delta(\frac{Q^2}{2m_\chi} - v_\chi Q\cos\theta + \omega)\end{aligned} \tag{2.73}$$

where θ is the angle between the velocity of the incoming dark matter particle, $\mathbf{v}_\chi$, and the transmitted momentum, $\mathbf{Q}$. By converting to spherical coordinates for the d^3Q-integral with the z-axis along $\mathbf{v}_\chi$, the expression for Γ become

$$\begin{aligned}\Gamma(v_\chi) = \int d\omega \int_0^{2\pi} d\varphi \int_{-1}^{1} d(\cos\theta) \int \frac{dQQ^2}{(2\pi)^3} \frac{\pi\bar{\sigma}_e}{\mu_{\chi e}^2} \\ \Big(\frac{\alpha m_e^2 + m_{A'}^2}{Q^2 + m_{A'}^2}\Big)^2 \frac{(-2)\mathrm{Im}(\chi_{\rho\rho}(\omega, Q))}{1 - e^{-\beta\omega}} \delta(\frac{Q^2}{2m_\chi} - v_\chi Q\cos\theta + \omega) = \\ \int d\omega \int_{-1}^{1} d(\cos\theta) \int \frac{dQQ}{(2\pi)^2} \frac{\pi\bar{\sigma}_e}{v_\chi \mu_{\chi e}^2} \Big(\frac{\alpha m_e^2 + m_{A'}^2}{Q^2 + m_{A'}^2}\Big)^2 \\ \frac{(-2)\mathrm{Im}(\chi_{\rho\rho}(\omega, Q))}{1 - e^{-\beta\omega}} \delta(\frac{Q}{2m_\chi v_\chi} + \frac{\omega}{Q v_\chi} - \cos\theta).\end{aligned} \tag{2.74}$$

The kinematic requirement for the scattering process in the above expression can also be expressed in terms of the Heaviside-step functions, θ,

$$\int_{-1}^{1} d(\cos\theta)\delta(\frac{Q}{2m_\chi v_\chi} + \frac{\omega}{Q v_\chi} - \cos\theta) = \theta(v_\chi - v_{\min}(\omega, Q))\theta(v_\chi + v_{\min}(\omega, Q)) \tag{2.75}$$

where $v_{\min}$ is given by

$$v_{\min} = \frac{Q}{2m_\chi} + \frac{\omega}{Q}. \tag{2.76}$$

Using this formulation of the kinematic requirement the expression for the scattering rate, Γ, is given by

$$\begin{aligned}\Gamma(v_\chi) = \int d\omega \int \frac{dQQ}{(2\pi)^2} \frac{\pi\bar{\sigma}_e}{v_\chi \mu_{\chi e}^2} \Big(\frac{\alpha m_e^2 + m_{A'}^2}{Q^2 + m_{A'}^2}\Big)^2 \\ \frac{(-2)\mathrm{Im}(\chi_{\rho\rho}(\omega, Q))}{1 - e^{-\beta\omega}} \theta(v_\chi - v_{\min}(\omega, Q))\theta(v_\chi + v_{\min}(\omega, Q)).\end{aligned} \tag{2.77}$$

Equivalently, the kinematic requirement can be expressed as integration limits according to

$$\Gamma(v_\chi) = \int_{-\infty}^{\frac{m_\chi v_\chi^2}{2}} d\omega \int_{Q_-}^{Q_+} \frac{dQQ}{(2\pi)^2} \frac{\pi\bar{\sigma}_e}{v_\chi \mu_{\chi e}^2} \Big(\frac{\alpha m_e^2 + m_{A'}^2}{Q^2 + m_{A'}^2}\Big)^2 \frac{(-2)\mathrm{Im}(\chi_{\rho\rho}(\omega, Q))}{1 - e^{-\beta\omega}} \tag{2.78}$$

where

$$Q_- = |m_\chi v_\chi - \sqrt{m_\chi^2 v_\chi^2 - 2m_\chi\omega}| \tag{2.79}$$

$$Q_+ = m_\chi v_\chi + \sqrt{m_\chi^2 v_\chi^2 - 2m_\chi\omega}. \tag{2.80}$$

Notice that these limits assume non-relativistic velocities of the dark matter particles. As discussed in Section 2.4, the in-medium effect affecting the reaction rate is packed into the density-density response function, $\chi_{\rho\rho}$.

Now, to show the effect of the medium on the scattering rate, we will start with only including the electrons in the in-medium effect. In the limit of heavy mediator Figure 2.2 compares the case where screening is included to the unscreened case. Note that no screening simply corresponds to $|\varepsilon|$ being set to one in Equation (2.59). This is done in the conditions present around the radial position $r = 0.1R_\odot$ where the number density, n_e, is $4.0 \cdot 10^{25}$ cm^{-3} and the temperature, T, is $1.3 \cdot 10^7$ K according to the solar model presented in Appendix C. Furthermore, these comparisons use an incoming dark matter velocity v_χ of 0.0044, reference cross section $\bar{\sigma}_e = 10^{-38}$ cm^2 and dark matter masses between 0.01 MeV to 10 MeV.

Notice in Figure 2.2 that the in-medium effects are most prominent for the lighter dark matter particles. It is also worth noting that the difference between the screened and unscreened cases is most important around small energy transfers, while for larger energy transfers the in-medium effects are less prominent. These features are probably due to the factor of $\frac{1}{Q^2}$ from the Coulomb interaction, V_e. For higher masses or transferred energies, the allowed transferred momenta also get larger, which leads to V_e suppressing the in-medium effects.

Due to the extra factor of $\frac{1}{Q^4}$ occurring in the light mediator limit the unscreened case has a singularity for interactions where the transferred energy, ω, is zero since, for zero transferred energy, the kinematic requirement allows Q to become zero. Therefore, in the limit of light mediator, screening has to be taken into account to obtain reasonable results. For this reason, the comparison in Figure 2.3 is not between the case of no screening and screening. In these Figures, the comparison is instead between screening using the Π_e from Equation (2.57) and screening using the low energy and momentum approximation for Π_e from Equation (2.66). The comparisons were performed under the same conditions as for the heavy mediator case.

One important feature in the plots in Figure 2.3 is that, generally, the difference between the two expressions for screening is most prominent for interactions with energy transfers around zero. Considering that the approximation should work best

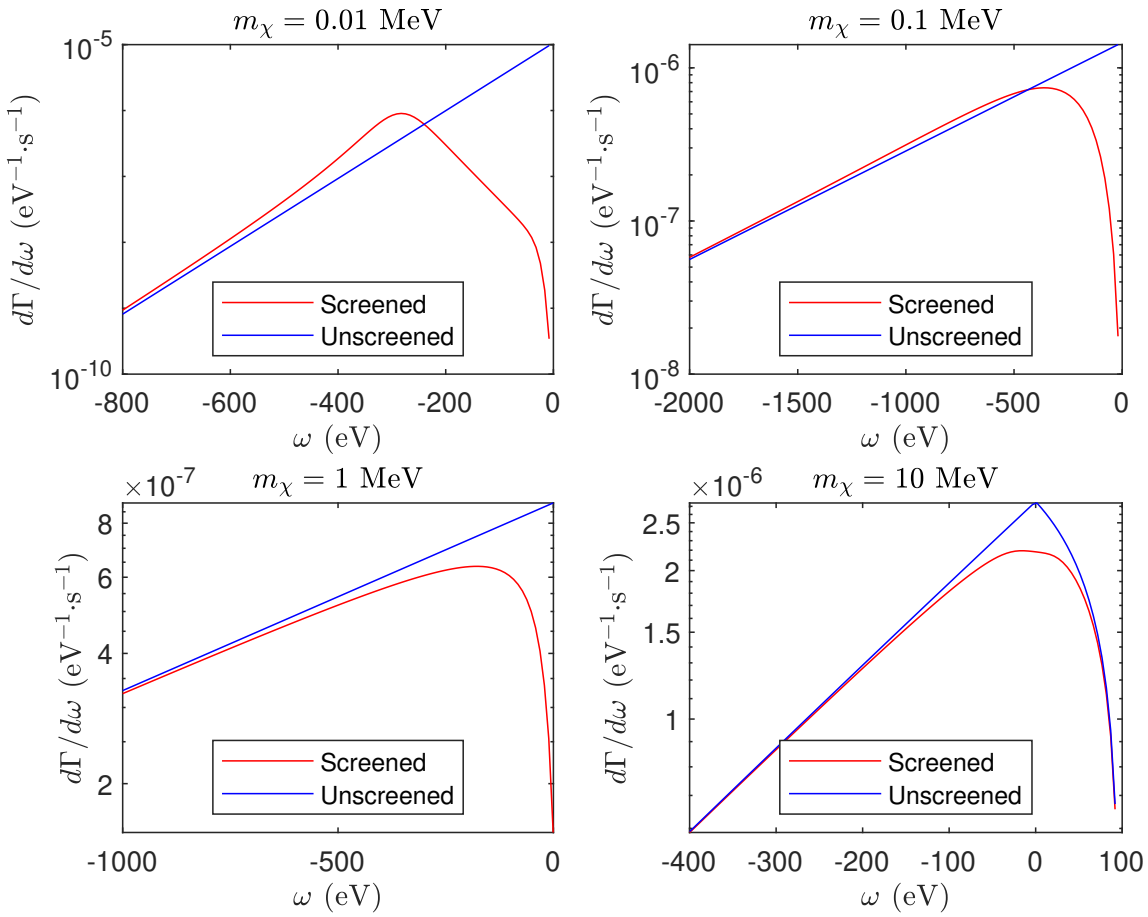

Figure 2.2: Comparison between the case of screened and unscreened interaction rate between dark matter and solar medium in the limit of a heavy mediator for dark matter masses, m_χ, between 0.01 MeV and 10 MeV. The calculations were made in the conditions present around $0.1R_\odot$ and the velocity of the incoming dark matter particle was set to 0.0044.

for small energy and momentum transfers, this feature warrants an explanation. First of all, the reason for the discrepancy around zero transferred energy could be caused by the fact that even for small energy transfers the momentum transfers are still allowed to reach finite values, causing the approximation to deviate. Secondly, the reason for the two versions of scattering rates to still approach similar values for larger energy transfers, even though the approximated screening should be worse there, might be that for this region the screening effects are undermined by the factor of $\frac{1}{Q^2}$ from V_e.

Comparing the screened scattering rates in Figures 2.2 and 2.3 show that, in general, for the light mediator limit most interactions take place around zero transferred energy while, especially for the lighter dark matter masses, interactions around zero transferred energy are heavily suppressed in the heavy mediator limit. On the other hand, scatterings occurring with higher transferred energies are more likely to occur

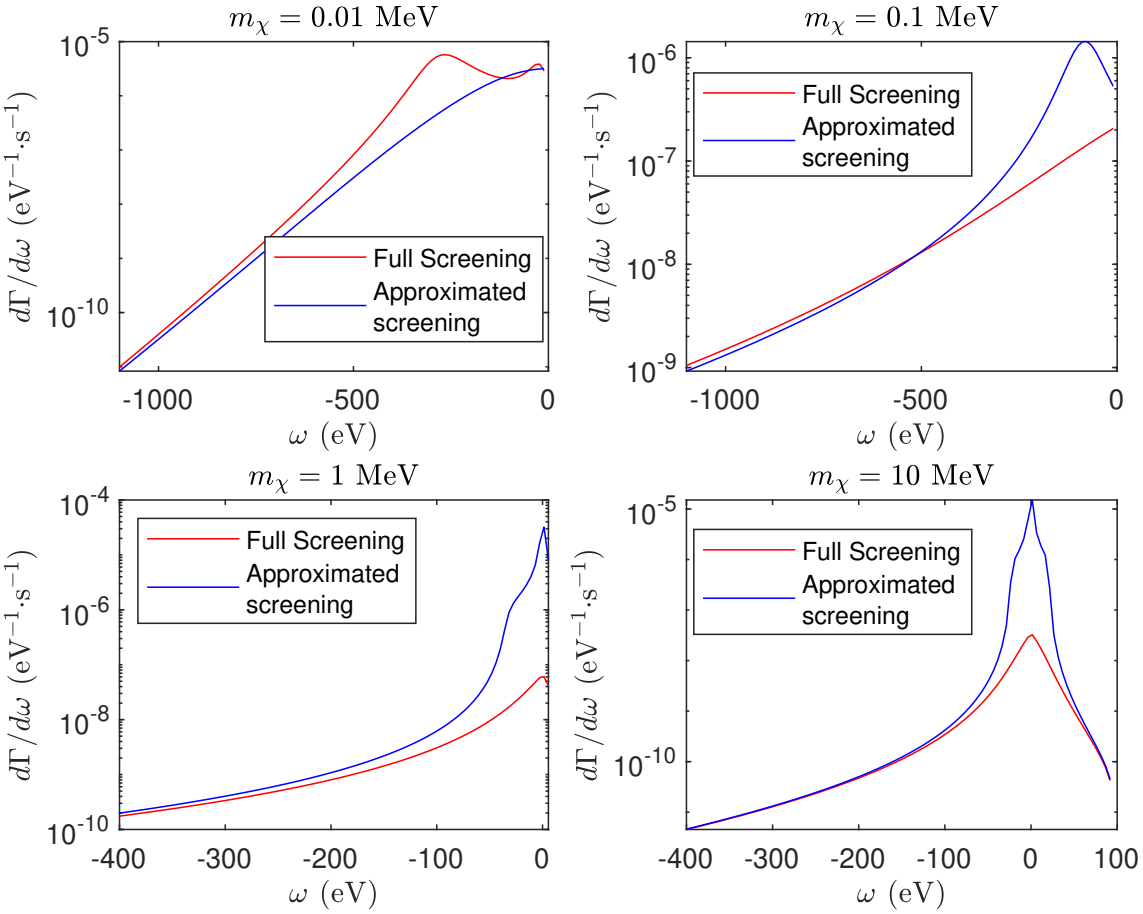

Figure 2.3: Comparison between the case of screened interaction rate between dark matter and solar-medium using the Π_e in Equation (2.57) and the approximated Π_e in Equation (2.66) in the limit of a light mediator for dark matter masses, m_χ, between 0.01 MeV and 10 MeV. The calculations were made in the conditions present around $0.1R_\odot$ and the velocity of the incoming dark matter particle was set to 0.0044.

within the heavy mediator limit. These differences should come from the factor of $\frac{1}{Q^4}$ since that is the only difference between the two cases.

So far in Figures 2.2 and 2.3 the in-medium effect is assumed to only come from the electrons. The ions of the medium can, as outlined in Section 2.4.1, be included using the expression in Equation (2.71) for the density-density response function, $\chi_{\rho\rho}$. In Figures 2.4 and 2.5 the effect of the ions also being included in the screening is compared to the case of screening from only the electrons for heavy and light mediators respectively. For the calculations, the Sun is approximated to consist of 75% Hydrogen and 25% Helium where the respective number densities n_{H} and n_{He} are calculated from the electron number density, n_e, by assuming charge neutrality. The calculations were performed in the same conditions as before around the radial position $r = 0.1R_\odot$ and for the dark matter mass, $m_\chi = 1$ MeV.

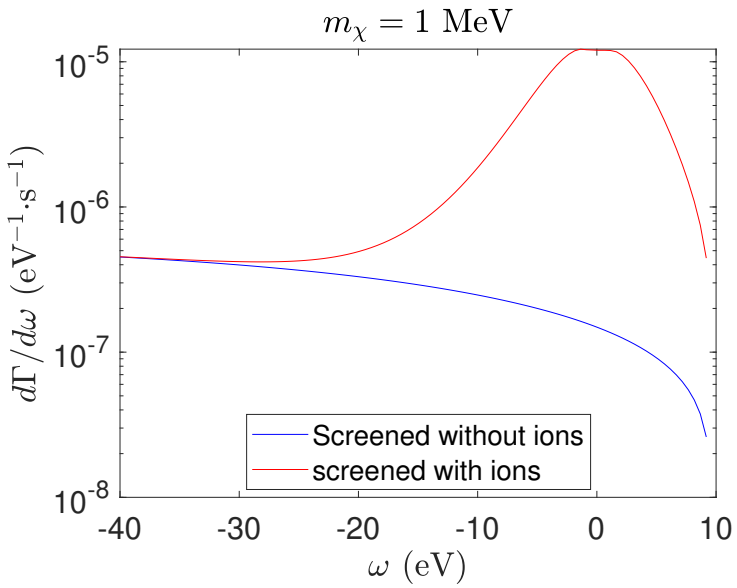

Figure 2.4: Comparison between the in-medium effects from just the electrons and the in-medium effects also taking into account the ions of the medium in the heavy mediator limit.

The perhaps most important features to observe in Figures 2.4 and 2.5 are that the inclusion of ions in the in-medium effect only has a significant effect on the scattering rate around zero transferred energy. Also note that, for the light mediator case, the inclusion of the ions increases the scattering rate with several orders of magnitude around zero, while, for the heavy mediator case, the ions only increase the scattering rate with about one order of magnitude around zero. These enhancements of the scattering rates around zero transferred energy most likely stem from the factors of V_e, each containing a factor $\frac{1}{Q^2}$, in some of the terms in Equation (2.71). In the heavy mediator limit the denominator of Equation (2.71) still contains enough of these factors of $\frac{1}{Q}$ to compensate but in the light mediator limit the extra factor of $\frac{1}{Q^4}$ causes the divergence seen in Figure 2.5. The reason why the inclusion of the ions in the medium is less important further away from zero transferred energy is probably because Π_N from Equation (2.69) approaches zero much faster compared to Π_e from Equation (2.57) due to the ions being far heavier than the electrons. If Π_N can be approximated to zero, the expressions for the imaginary part of the density-density response function when including the ions, Equation (2.71), and ignoring the ions, Equation (2.59), coincide.

As a final remark, it is important to note that the results presented in Figures 2.2, 2.3, 2.4 and 2.5 agree with the results presented in Ref. [45]. In this thesis, we have performed the calculations at slightly different solar conditions and initial dark matter velocities, but the results still look similar. Considering the relatively small variations in solar conditions and initial velocities compared to [45], these similarities should be reasonable.

Now that the scattering rate has been computed, it can be utilised to elucidate the

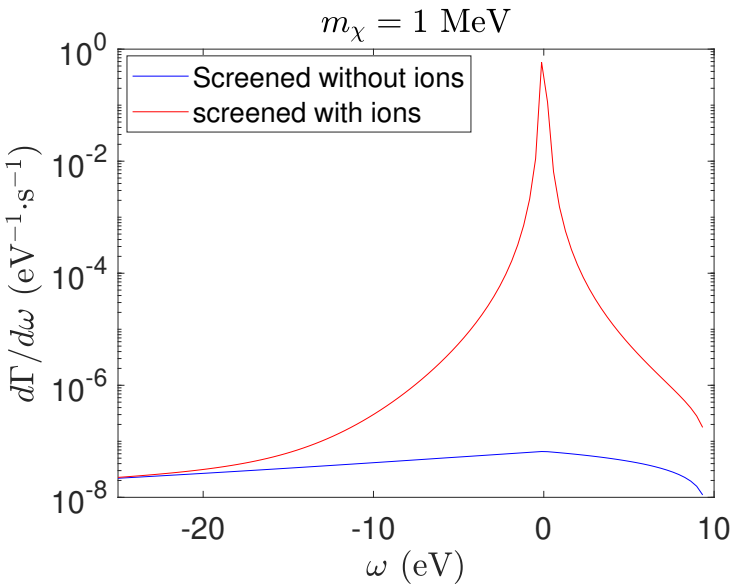

Figure 2.5: Comparison between the in-medium effects from just the electrons and the in-medium effects also taking into account the ions of the medium in the light mediator limit.

behaviours of some potential observables. This will be the focus of the coming two chapters where we will implement the scattering rate computed in this chapter to the phenomena of solar dark matter capture and solar dark matter reflection.

3

Dark Matter Capture in a Sun-like Celestial Body

The first possible observable related to solar dark matter interactions that we will investigate in this thesis is connected to solar dark matter capture. Here, the idea is that if dark matter could get gravitationally bound inside the Sun that could be a region of high dark matter density. Under this assumption, there could be a chance of detecting signals from these particles interacting with each other, for example via the products of them annihilating [51].

This chapter will, largely, be based on section 3 of Ref. [51]. However the expression used for the scattering rate, Γ, will look slightly different since the authors of that article do not use linear response theory in their calculation.

The overarching idea is that an infalling dark matter particle with energy E inside the star had energy $E_\infty = \sqrt{B}E$ in the halo before being gravitationally accelerated by the star. If the phase space density of the dark matter in the halo, $f_\infty(E_\infty)$, is assumed to be isotropically distributed, the phase space density in the star is set by $f(E) = f_\infty(\sqrt{B}E)$ since the phase space density is preserved during infall due to Liouville's theorem. The expression for f_∞ can be related to the velocity distribution of the halo dark matter, p_v, by noting

$$\begin{aligned} n_\chi = g_s \int \frac{d^3p}{(2\pi)^3} f_\infty = \frac{g_s m_\chi^3}{(2\pi)^3} \int d^3v f_\infty \implies \\ \{\int d^3v p_v = 1\} \implies f_\infty(p) = \frac{(2\pi)^3 n_\chi}{g_s m_\chi^3} p_v(\frac{p}{m_\chi}) \end{aligned} \tag{3.1}$$

where the halo dark matter is assumed to be non-relativistic, n_χ is the number density of the halo dark matter and g_s is the spin degeneracy. For notational convenience $\hat{f}_\infty$ is defined as

$$\hat{f}_\infty \equiv \frac{g_s}{(2\pi)^3} f_\infty. \tag{3.2}$$

Given this, the capturing rate, C, per unit volume inside the star is given by

$$\frac{C}{V} = \int d^3p \hat{f}(p) \Gamma_{E \to E' < E_{\text{esc}}} \tag{3.3}$$

where $\Gamma_{\mathrm{E}\to\mathrm{E}'<\mathrm{E}_{\mathrm{esc}}}$ denote the rate of scatterings that bring the dark matter from a gravitationally unbound to a gravitationally bound energy. Assuming the isotropic distribution of the dark matter and making the variable substitution $E = \sqrt{m_\chi^2 + p^2}$, leading to $dp = \frac{E}{p}dE$, the capture rate per volume can be expressed

$$\begin{aligned}\frac{C}{V} = 4\pi \int dp p^2 \hat{f}(p)\Gamma_{E\to E'<E_{\mathrm{esc}}} = 4\pi \int dE E p \hat{f}(E)\Gamma_{E\to E'<E_{\mathrm{esc}}} = \\ 4\pi \int dE E \sqrt{E^2 - m_\chi^2}\hat{f}(E)\Gamma_{E\to E'<E_{\mathrm{esc}}}.\end{aligned} \tag{3.4}$$

Since, for capture, the initial energies that are of interest are those that are not already bound the lower integration limit should be set to $E_{\mathrm{esc}} = \frac{m_\chi}{\sqrt{B}}$, leading to

$$\begin{aligned}\frac{C}{V} = 4\pi \int_{\frac{m_\chi}{\sqrt{B}}}^{\infty} dE E^2 \sqrt{1 - \frac{m_\chi^2}{E^2}}\hat{f}(E)\Gamma_{E\to E'<E_{\mathrm{esc}}} = \\ 4\pi \frac{1}{B^{3/2}} \int_{m_\chi}^{\infty} dE_\infty E_\infty^2 \sqrt{1 - \frac{m_\chi^2 B}{E_\infty^2}}\hat{f}_\infty(E_\infty)\Gamma_{E\to E'<E_{\mathrm{esc}}}.\end{aligned} \tag{3.5}$$

Although the integral in the above expression has an upper bound at infinite energy, i.e. relativistic energy, the distribution $\hat{f}_\infty(E_\infty)$ ensures that the relevant range of the integral is well below relativistic energies, again assuming non-relativistic halo dark matter. Given this property of non-relativistic energy $E_\infty \approx m_\chi$ we get

$$\frac{C}{V} \approx 4\pi \frac{\sqrt{1-B}}{B^{3/2}} m_\chi^2 \int_{m_\chi}^{\infty} dE_\infty \hat{f}_\infty(E_\infty)\Gamma_{E\to E'<E_{\mathrm{esc}}}, \tag{3.6}$$

this is the capture rate per unit volume observed by an observer in the star, where $B < 1$, however for an observer at infinity, where $B = 1$, the capture rate will be observed as

$$C = 4\pi m_\chi^2 \int dV \frac{\sqrt{1-B}}{B} \int_{m_\chi}^{\infty} dE_\infty \hat{f}_\infty(E_\infty)\Gamma_{E\to E'<E_{\mathrm{esc}}}. \tag{3.7}$$

Using the expression for the scattering rate from Equation (2.78) the capture rate looks like

$$\begin{aligned}C = 4\pi m_\chi^2 \int dV \frac{\sqrt{1-B}}{B} \int_{m_\chi}^{\infty} dE_\infty \hat{f}_\infty(E_\infty) \int_{\frac{E_\infty - m_\chi}{\sqrt{B}}}^{\frac{m_\chi v_\chi^2}{2}} d\omega \\ \int_{Q_-}^{Q_+} \frac{dQQ}{(2\pi)^2} \frac{\pi\bar{\sigma}_e}{v_\chi \mu_{\chi e}^2} \Big(\frac{\alpha m_e^2 + m_{A'}^2}{Q^2 + m_{A'}^2}\Big)^2 \frac{(-2)\mathrm{Im}(\chi_{\rho\rho}(\omega, Q))}{1 - e^{-\beta\omega}}\end{aligned} \tag{3.8}$$

where the lower limit on the energy, ω, integral comes from the requirement of $E \to E' < E_{\mathrm{esc}}$. Assuming that the escape velocity, i.e. the velocity that the dark matter particle has gained during infall, is sufficiently larger than typical halo dark matter velocities, further simplifications can be made to the expression for the capture rate. In that case, Q and ω only depend weakly on E_∞, since most of the

energy and momentum has been gained during the infall and $v_\chi \approx v_{\text{esc}} = \sqrt{1-B}$, which leads to

$$C \approx \frac{\bar{\sigma}_e m_\chi^2}{\mu_{\chi e}^2} \int dV \frac{1}{B} \int_{m_\chi}^{\infty} dE_\infty \hat{f}_\infty(E_\infty) \int_{\frac{E_\infty - m_\chi}{\sqrt{B}}}^{\frac{m_\chi v_\chi^2}{2}} d\omega \int_{Q_-}^{Q_+} dQQ\Big(\frac{\alpha m_e^2 + m_{A'}^2}{Q^2 + m_{A'}^2}\Big)^2 \frac{(-2)\text{Im}(\chi_{\rho\rho}(\omega, Q))}{1 - e^{-\beta\omega}}. \tag{3.9}$$

The escape velocity at a radius r inside the Sun, where the Schwarzschild framework is no longer valid, is given by

$$v_{\text{esc}}(r) = \sqrt{\frac{2G_N M_\odot}{R_\odot}\left(1 + \frac{R_\odot}{M_\odot}\int_r^{R_\odot} dr' \frac{M_\odot(r')}{r'^2}\right)} \tag{3.10}$$

where $M_\odot(r')$ denotes the amount of solar mass that is inside the radius r' obtained from the solar model presented in Appendix C and G_N is the gravitational constant [54]. Outside the Sun, the escape velocity simply reduces to

$$v_{\text{esc}}(r) = \sqrt{\frac{2G_N M_\odot}{r}} \tag{3.11}$$

according to the Schwarzschild metric.

In the scenario where most of the kinetic energy of the dark matter particle is gained during the gravitational infall, it is also possible to swap places between the integrals over E_∞ and ω in Equation (3.9), using $E_k = E_\infty - m_\chi$,

$$\begin{aligned}\int_{m_\chi}^{\infty} dE_\infty \hat{f}_\infty(E_\infty) \int_{\frac{E_\infty - m_\chi}{\sqrt{B}}}^{\frac{m_\chi v_\chi^2}{2}} d\omega = \int_0^{\infty} dE_k \hat{f}_\infty(E_k + m_\chi) \int_{\frac{E_k}{\sqrt{B}}}^{\frac{m_\chi v_\chi^2}{2}} d\omega \approx \\ \int_0^{\frac{m_\chi v_\chi^2}{2}} d\omega \int_0^{\sqrt{B}\omega} dE_k \hat{f}_\infty(E_k + m_\chi) \equiv \int_0^{\frac{m_\chi v_\chi^2}{2}} d\omega \hat{F}_\infty(\sqrt{B}\omega)\end{aligned} \tag{3.12}$$

and therefore

$$C \approx \frac{\bar{\sigma}_e m_\chi^2}{\mu_{\chi e}^2} \int dV \frac{1}{B} \int_0^{\frac{m_\chi v_\chi^2}{2}} d\omega \hat{F}_\infty(\sqrt{B}\omega) \int_{Q_-}^{Q_+} dQQ\Big(\frac{\alpha m_e^2 + m_{A'}^2}{Q^2 + m_{A'}^2}\Big)^2 \frac{(-2)\text{Im}(\chi_{\rho\rho}(\omega, Q))}{1 - e^{-\beta\omega}}. \tag{3.13}$$

Note that for the Sun, where the escape velocity in general is non-relativistic the value for B is close to 1. This means that a further simplification can be made according to

$$C \approx \frac{\bar{\sigma}_e m_\chi^2}{\mu_{\chi e}^2} \int dV \int_0^{\frac{m_\chi v_\chi^2}{2}} d\omega \hat{F}_\infty(\omega) \int_{Q_-}^{Q_+} dQQ\Big(\frac{\alpha m_e^2 + m_{A'}^2}{Q^2 + m_{A'}^2}\Big)^2 \frac{(-2)\text{Im}(\chi_{\rho\rho}(\omega, Q))}{1 - e^{-\beta\omega}}. \tag{3.14}$$

Assuming the halo dark matter to follow an offset Maxwell velocity distribution, where the offset comes from the fact that the Sun is moving through the galaxy, the function $\hat{F}_\infty$ can be calculated via

$$F_\infty(\delta) \equiv \int_0^\delta dE_k f_\infty(m_\chi + E_k) = m_\chi \int_0^{v_\delta} dv v f_\infty(m_\chi v) \tag{3.15}$$

where v_δ is such that $\frac{m_\chi v_\delta^2}{2} = \delta$. By assuming an of isometric distribution we get

$$F_\infty(\delta) = \frac{m_\chi}{4\pi} \int_0^{v_\delta} d^3v \frac{f_\infty(m_\chi v)}{v} = \frac{2\pi^2 n_\chi}{g_s m_\chi^2} \int_0^{v_\delta} d^3v \frac{p_v(v)}{v} \tag{3.16}$$

and the offset velocity distribution is given by

$$p_v(v) = (2\pi v_0^2)^{-3/2} \exp\left(-\frac{(v - v_*)^2}{2v_0^2}\right) \tag{3.17}$$

where $v_0 \approx 0.0007$ is the velocity dispersion of the halo dark matter and $v_* \approx 0.0007$ is the velocity of the star. The function $F_\infty(\delta)$ can be calculated according to

$$\begin{aligned} F_\infty(\delta) = \frac{2\pi^2 n_\chi}{g_s m_\chi^2}(2\pi v_0^2)^{-3/2} 2\pi \int_{-1}^{1} d(\cos\theta) \int_0^{v_\delta} dv v \exp\left(-\frac{1}{2v_0^2}(v^2 + 2vv_* \cos\theta + v_*^2)\right) = \\ \frac{4\pi^3 n_\chi}{g_s m_\chi^2}(2\pi v_0^2)^{-3/2} \int_0^{v_\delta} dv v \exp\left(-\frac{v^2 + v_*^2}{2v_0^2}\right) \int_{-1}^{1} d\cos\theta \exp\left(\frac{vv_*}{v_0^2}\cos\theta\right) = \\ \frac{4\pi^3 n_\chi}{g_s m_\chi^2}(2\pi v_0^2)^{-3/2} \int_0^{v_\delta} dv \frac{v_0^2}{v_*} \exp\left(-\frac{v^2 + v_*^2}{2v_0^2}\right) \left[\exp\left(\frac{vv_*}{v_0^2}\cos\theta\right)\right]_{-1}^{1} = \\ \frac{4\pi^3 n_\chi}{g_s m_\chi^2}(2\pi v_0^2)^{-3/2} \int_0^{v_\delta} dv \frac{v_0^2}{v_*} \exp\left(-\frac{v^2 + v_*^2}{2v_0^2}\right) \left(\exp\left(\frac{vv_*}{v_0^2}\right) - \exp\left(-\frac{vv_*}{v_0^2}\right)\right). \end{aligned} \tag{3.18}$$

Notice that a more accurate velocity distribution would also implement a cutoff at the galactic escape velocity, however, due to the factor of $\frac{1}{v}$ in Equation (3.16) this can be neglected without any significant consequences [51]. Calculating the two terms in the last line of Equation (3.18) separately leads to

$$\int_0^{v_\delta} dv \frac{v_0^2}{v_*} \exp\left(-\frac{1}{2v_0^2}(v^2 - 2vv_* + v_*^2)\right) = \frac{\sqrt{\pi} v_0^3}{\sqrt{2} v_*} \left(\operatorname{erf}\left(\frac{v_\delta - v_*}{\sqrt{2}v_0}\right) + \operatorname{erf}\left(\frac{v_*}{\sqrt{2}v_0}\right)\right) \tag{3.19}$$

$$\int_0^{v_\delta} dv \frac{v_0^2}{v_*} \exp\left(-\frac{1}{2v_0^2}(v^2 + 2vv_* + v_*^2)\right) = \frac{\sqrt{\pi} v_0^3}{\sqrt{2} v_*} \left(\operatorname{erf}\left(\frac{v_\delta + v_*}{\sqrt{2}v_0}\right) - \operatorname{erf}\left(\frac{v_*}{\sqrt{2}v_0}\right)\right) \tag{3.20}$$

which implies

$$F_\infty(\delta) = \frac{\pi^2 n_\chi}{g_s m_\chi^2 v_*} \left(2\operatorname{erf}\left(\frac{v_*}{\sqrt{2}v_0}\right) + \operatorname{erf}\left(\frac{v_\delta - v_*}{\sqrt{2}v_0}\right) - \operatorname{erf}\left(\frac{v_\delta + v_*}{\sqrt{2}v_0}\right)\right). \tag{3.21}$$

Note that with $\delta = \omega$ the expression for v_δ is given by $v_\delta = \sqrt{\frac{2\omega}{m_\chi}}$. Using this the expression for the capture rate in Equation (3.14) can be rewritten

$$C \approx \frac{\bar{\sigma}_e n_\chi}{8\pi v_* \mu_{\chi e}^2} \int dV \int_0^{\frac{m_\chi v_\chi^2}{2}} d\omega \left(2\text{erf}\left(\frac{v_*}{\sqrt{2}v_0} \right) + \text{erf}\left(\frac{\sqrt{\frac{2\omega}{m_\chi}} - v_*}{\sqrt{2}v_0} \right) \right.$$
$$\left. -\text{erf}\left(\frac{\sqrt{\frac{2\omega}{m_\chi}} + v_*}{\sqrt{2}v_0} \right) \right) \int_{Q_-}^{Q_+} dQQ \left(\frac{\alpha m_e^2 + m_{A'}^2}{Q^2 + m_{A'}^2} \right)^2 \frac{(-2)\text{Im}(\chi_{\rho\rho}(\omega, Q))}{1 - e^{-\beta\omega}}. \tag{3.22}$$

3.1 Capture rate

When looking into dark matter capture it is important to note that the available phase space for capture is quite small for the masses most affected by the in-medium effects; see Figures 2.2 and 2.3. These plots assumed that the incoming dark matter particles had the velocity according to the relevant escape velocity for that particular radial position inside the Sun, using Equation (3.10). For such a velocity and for the masses where the in-medium effects are most prominent, it is clear that the phase space for capture is quite small since the relevant regime for this is the part with $\omega > 0$. For heavier dark matter particles, this phase space increases, but for those masses the in-medium effects are not as prominent.

In Figure 3.1 the expression for the capture rate in Equation (3.22) is plotted as a function of the reference cross section, $\bar{\sigma}_e$, and dark matter mass, m_χ, in the heavy mediator limit. Notice that, since the regime of small energy transfers is of interest, the integral over ω in Equation (3.22) goes from zero. The expression for the density-density response function that should be used for valid results is the one also considering the ions from Equation (2.71).

Notice in Figure 3.1 how the capture rate increases with the reference cross section, $\bar{\sigma}_e$, which is to be expected since $\bar{\sigma}_e$ only enters as a scaling factor in Equation (3.22). Furthermore, the capture rate increases with the dark matter mass, m_χ, which is also reasonable since the available phase space for capture increases for larger dark matter masses due to the integration bound $\frac{m_\chi v_\chi^2}{2}$ in Equation (3.22).

For the light mediator limit, a similar procedure can be performed. However, due to the extra factor of $\frac{1}{Q^4}$, the scattering rate becomes huge around zero transferred energy, see Figure 2.5. Therefore, to prevent this issue in the light mediator limit, we introduce a cutoff, $\nu = 10^{-4}$ eV, on the lower limit of the ω-integral in Equation (3.22). Interactions with lower values of transferred energy could still capture the dark matter particle. Even for the lowest dark matter mass treated here, $m_\chi = 0.01$ MeV, and the escape velocity at the edge of the Sun, ≈ 0.0021, the escape energy is ≈ 20 meV. Therefore, this cutoff only disregards the regime of captured particles that have energies close to the unbound regime. In Figure 3.2 the expression for the capture rate in Equation (3.22), with a cutoff on the ω-integral $\nu = 10^{-4}$ eV, is plotted as a function of the reference cross section, $\bar{\sigma}_e$, and dark matter mass, m_χ,

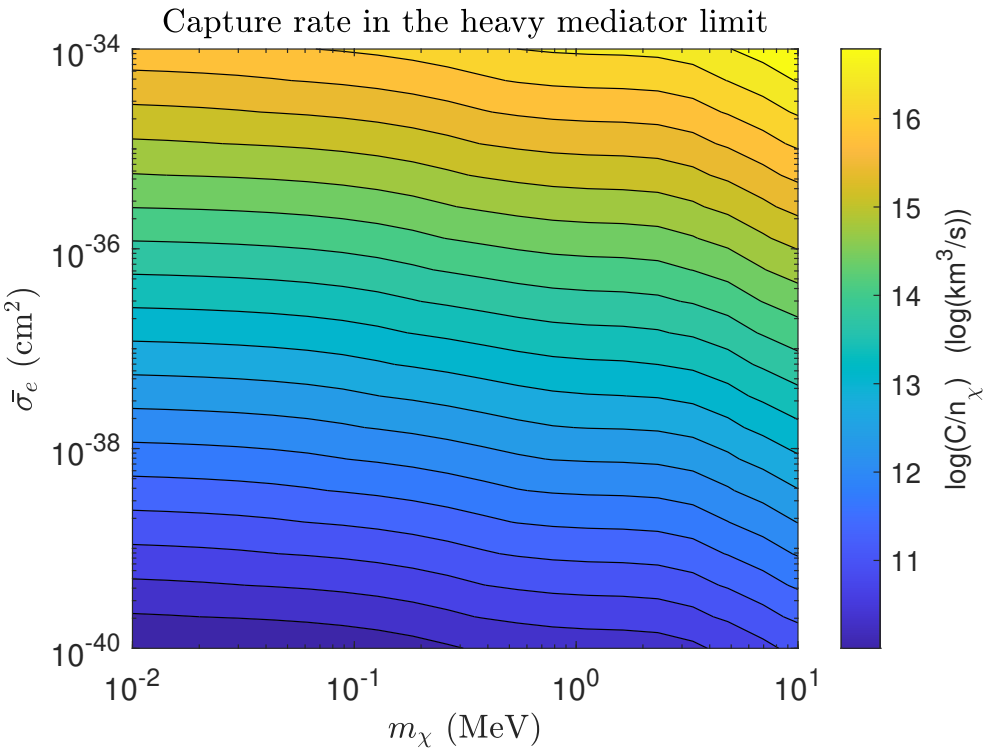

Figure 3.1: The rate at which dark matter particles undergo scatterings causing them to get gravitationally bound to the Sun in the heavy mediator limit as a function of the reference cross section, σ_e, and dark matter mass, m_χ.

in the light mediator limit.

Notice in Figure 3.2 how, similarly to the situation in the heavy mediator limit shown in Figure 3.1, the capture rate increases with the reference cross section, $\bar{\sigma}_e$, as expected. However, one should note that for the light mediator case, displayed in Figure 3.2, the highest capture rate is obtained for the lower masses, despite their lack of phase space mentioned above. The reason for this could come from the kinematic requirement, which for these low masses allows for the transferred momenta to become quite small, despite the cutoff. Therefore, the factor of $\frac{1}{Q^4}$ helps to increase the capture rate drastically. Another important difference between the situation in Figure 3.1 and the situation in Figure 3.2 is that for the light mediator case, the capture rate is several orders of magnitude larger compared to the heavy mediator case. This was also expected since the energy region of interest lies relatively close to zero where the light mediator limit gives a much larger scattering rate.

As a final remark on the subject of dark matter capture, it is important to still keep in mind how, as suggested by the plots in Figures 2.2, 2.3, 2.4 and 2.5, the rate of scatterings occurring where the dark matter gains energy is far greater than the rate of capture for the masses treated in this thesis. Furthermore, one should note that even in the cases where the initial scattering event is such that the particle gets

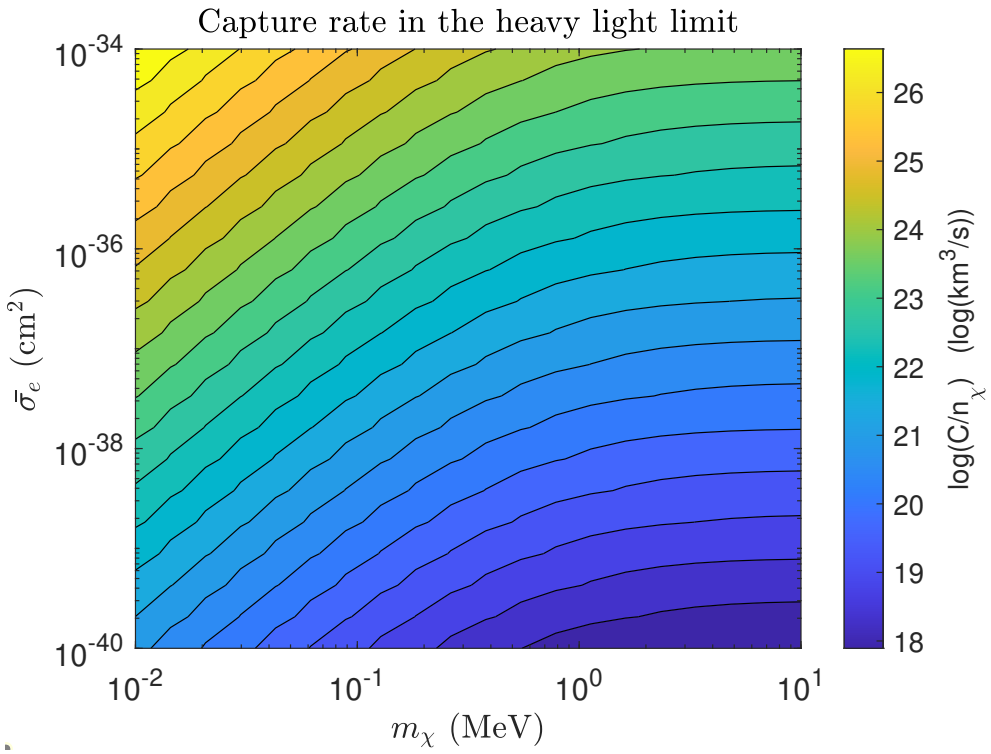

Figure 3.2: The rate at which dark matter particles undergo scatterings causing them to get gravitationally bound to the Sun in the light mediator limit as a function of the reference cross section, σ_e, and dark matter mass, m_χ.

captured, it could still be possible for that particle to undergo further interactions where it gains energy, thus becoming unbound yet again. Simulations would have to be performed to further elucidate these scenarios, but this has not been done in this work. The scenario of dark matter reflection, where the dark matter gains energy in its interaction with the Sun, however, will be treated in the next chapter.

4

Reflection of Dark Matter in the Sun

The focus in this chapter will lie on solar dark matter reflections, meaning that the dark matter gains energy when interacting with the Sun. The potential observational benefit of this is that some dark matter particles arriving here on Earth might have significantly higher energies compared to dark matter particles arriving without first interacting with the Sun due to them being reflected by the Sun. This possibility of having access to some incoming dark matter particles with higher energy could have some importance in direct detection experiments [52, 54, 55]. Note however that in this report we will restrict ourselves to looking at the solar interactions, omitting discussions about how this might affect direct detection endeavours.

This chapter is largely based on Refs. [52, 54], however in this thesis, we will also take into account the in-medium effects using the previously calculated scattering rate within the framework of linear response theory given in Equation (2.78). In this chapter, the used convention is that positive ω means that the dark matter particle has gained energy. Assuming at most single scattering in the Sun, the probability of a scattering event occurring with the transferred energy, ω, is given by

$$\left.\frac{dP}{d\omega}\right|_{\text{trajectory}} = \int_{\text{trajectory}} \frac{dl}{v_\chi}\frac{d\Gamma}{d\omega} \tag{4.1}$$

where the trajectory of the dark matter in the Sun is determined by the gravitational influence on the dark matter particle, its initial velocity, v_i, and impact parameter, R. It is important to note that the differential scattering rate, $\frac{d\Gamma}{d\omega}$, depends on what radius the dark matter particle is inside the Sun, since the temperature, T, and the number density of electrons, n_e, inside the Sun depends on the radius. The specific values for these variables were obtained from the solar model presented in Appendix C. Using the probability of scattering obtained in (4.1) the normalised kinetic energy distribution of the outgoing dark matter particle per unit of energy can be expressed as, assuming that the transferred energy is much higher than the incoming kinetic energy of the dark matter particle,

$$\frac{2}{R_{\text{max}}^2}\int_0^{R_{\text{max}}} dRR \int_0^{v_{\text{max}}} dv_i f_\chi(v_i) \left.\frac{dP}{d\omega}\right|_{\text{trajectory}} \tag{4.2}$$

where $R_{\max}$ is the maximum impact parameter chosen to be $4R_\odot$, v_i is the initial velocity of the dark matter in the halo and $v_{\max}$ is determined by the impact parameter to ensure that the dark matter particle passes through the Sun.

In Equation (4.2), $f_\chi(v_i)$ is the velocity distribution of the halo dark matter. This is similar to the distribution, p_v, presented in Equation (3.17), but here a cutoff Gaussian distribution is used

$$f_{\text{halo}}(\mathbf{v}_i) = \frac{1}{N_{\text{esc}}\pi^{3/2}v_0^3}\exp\left(-\frac{\mathbf{v}_i^2}{v_0^2}\right)\theta(v_{\text{gal}} - |\mathbf{v}_i|) \tag{4.3}$$

where the normalisation factor N_{esc} is given by

$$N_{\text{esc}} = \text{erf}\left(\frac{v_{\text{gal}}}{v_0}\right) - \sqrt{2}\sqrt{\pi}\frac{v_{\text{gal}}}{v_0}\exp\left(-\frac{v_{\text{gal}}^2}{v_0^2}\right). \tag{4.4}$$

The width of the Gaussian, v_0, is set to 0.007 and the galactic escape velocity, v_{gal}, is approximately 0.002 [52, 54]. To also take into account the Sun's movement through the galaxy, here assumed to have a velocity of about 0.0007, the velocity distribution of the halo dark matter as observed by the Sun, $f_{\text{obs}}(\mathbf{v})$, is given by

$$f_{\text{obs}}(\mathbf{v}_i) = f_{\text{halo}}(\mathbf{v}_i + \mathbf{v}_{\text{obs}}) \tag{4.5}$$

and therefore the expression for $f_\chi(v_i)$ that occurs in Equation (4.2) is given by

$$f_\chi(v_i) = \int d\Omega v_i^2 f_{\text{obs}}(\mathbf{v}_i). \tag{4.6}$$

4.1 The Dark Matter Particles Trajectory Inside the Sun Under the Influence of Gravity

To calculate the scattering rate, the trajectory of the dark matter particle moving through the Sun under the influence of gravity needs to be calculated. The procedure to do this is described in Ref. [54], but here, the most important points for these calculations will be highlighted. By fixing a coordinate system where the dark matter particle moves in a plane described by polar coordinates (r, ϕ) with the origin at the centre of the Sun, the equations of motion describing the particle trajectory are given by

$$0 = \ddot{r} - r\dot{\phi}^2 + \frac{G_N M_\odot(r)}{r^2} \tag{4.7}$$

$$J \equiv r^2\dot{\phi} = \text{constant} \tag{4.8}$$

where the dots denote a time derivative and where J is the angular momentum of the dark matter particle. Inside the Sun, where $M_\odot(r)$ varies depending on the radius, these equations need to be evaluated numerically and in this report, the Runge-Kutta-method has been utilised using the function ode45 in Matlab [56].

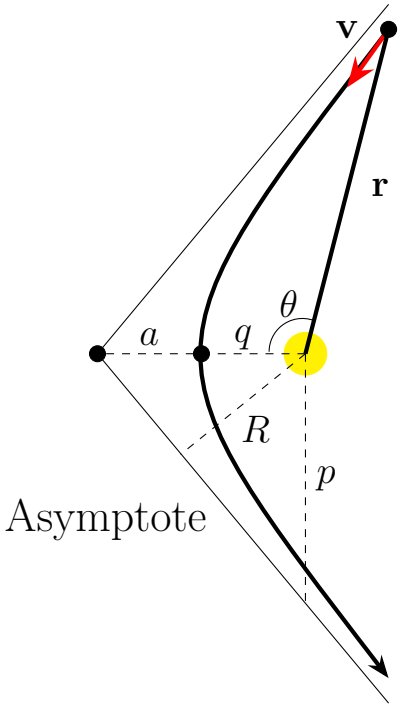

Figure 4.1: A schematic picture of a trajectory of a dark matter particle under the influence of gravity from the Sun. The most important geometric properties are highlighted, including the velocity of the particle, v, the radial position of the dark matter particle, r, the periapsis of the trajectory, q, the angle from periapsis, θ, the semimajor axis, a, the impact parameter R and the semilatus rectum, p.

Outside the Sun, for the propagation of the particle from far away to the edge of the Sun, the situation is somewhat simpler. For a schematic picture of the situation see Figure 4.1.

Notice how the trajectory in Figure 4.1 does not intersect with the Sun. However, the trajectories that will be of interest in this work have to intersect with the Sun typically meaning that they need to have a sufficiently small impact parameter and initial velocity. For these trajectories, analytical solutions of the particle's position and velocity at the edge of the Sun can be calculated given the impact parameter and initial velocity. These calculated properties can then be used as initial conditions when solving the equations of motion inside the sun given by equations (4.7) and (4.8). More specifically the initial conditions needed for those calculations are $r(0) = R_\odot$, $\phi(0) = 0$ and the initial radial velocity $v_r(0)$ obtained from the analytical calculations of the trajectory outside the Sun.

The perhaps most important parameter for the calculation of the trajectory is the angular momentum, J, of the particle that is given by the impact parameter, R, and the initial velocity, v_i, through the relation

$$J = Rv_i \tag{4.9}$$

since that is a conserved quantity throughout the trajectory, it is also true that

$J = |\mathbf{r} \times \mathbf{v}|$. The other important parameters of the trajectory are highlighted in Figure 4.1 where r and θ demonstrate the particle position in the plane that it is moving in and q is the periapsis of the trajectory. The other highlighted parameters in Figure 4.1 are, in analogy to Ref. [54], the semimajor axis, a, and the semilatus rectum, p, given by

$$a = \frac{G_N M_\odot}{v_i^2} \tag{4.10}$$

$$p = \frac{J^2}{G_N M_\odot}. \tag{4.11}$$

Using these parameters, another important feature of the trajectory, its eccentricity e, can be expressed according to

$$e = \sqrt{1 + \frac{p}{a}}. \tag{4.12}$$

To obtain the desired initial condition for the radial velocity, $v_r(0)$, the equations for position and velocity from Ref. [54] can be used. These state that the new angle from periapsis, θ', and the new velocity, v', can be expressed in terms of the new radial coordinate, r', which has to be equal to $R_\odot$ at the edge of the Sun. The expressions for θ' and v' respectively are given by

$$\theta' = \arccos\left(\frac{1}{e}\left(\frac{p}{r'} - 1\right)\right) \tag{4.13}$$

$$v' = \sqrt{\frac{G_N M_\odot}{p}}\sqrt{1 + e^2 + 2e\cos\theta'}. \tag{4.14}$$

The radial velocity at this point can be calculated from the observation that the angular momentum, J, must still be conserved and that $v' = v_\perp + v_\parallel$ where $v_\perp$ is perpendicular to the position vector and $|v_\parallel| = v_r(0)$. Using $J = R_\odot |v_\perp|$ implies that $|v_\perp| = \frac{v_i R}{R_\odot}$, which in turn implies that $v_r(0) = -\sqrt{v'^2 - \frac{v_i^2 R^2}{R_\odot^2}}$ where the minus sign comes from the fact that the particle has to travel towards smaller radial coordinates when entering the Sun.

The highest allowed initial velocity, $v_{\max}$ in Equation (4.2), given the impact parameter can now also be calculated. For impact parameters smaller than the radius of the Sun $v_{\max} = \infty$, but for impact parameters larger than the radius of the Sun, not all initial velocities are allowed. The angular momentum at periapsis, see Figure 4.1, is given by the velocity at periapsis times the radius the dark matter particle is at in that moment. The velocity at periapsis is given by

$$v_p(v_i, q) = \sqrt{v_i^2 + v_{\text{esc}}(q)^2} \tag{4.15}$$

where q is the distance from the centre at periapsis. To ensure that periapsis is inside the Sun we require that the angular momentum, J, obeys

$$J < R_\odot v_p(v_i, R_\odot), \tag{4.16}$$

which for the impact parameter, R, translates to

$$R < \sqrt{1 + \frac{v_{\text{esc}}(R_\odot)^2}{v_i^2}} R_\odot \tag{4.17}$$

or equivalently, given an impact parameter, sets the upper bound on the initial velocity, $v_{\max}$, to

$$v_{\max} = \frac{v_{\text{esc}}(R_\odot)}{\sqrt{\left(\frac{R}{R_\odot}\right)^2 - 1}}. \tag{4.18}$$

4.2 Single Scattering Limit

In this report, only the regime where single scatterings occur in the Sun will be dealt with. Processes with more than one scattering event per particle in the Sun would have to be investigated using simulations similar to Ref. [52]. For the considered scenario of only single scattering processes to be relevant, the total scattering probability, obtained by integrating the energy dependence in Equation (4.1), needs to be significantly smaller than one for typical trajectories in the Sun. The parameter that can be adjusted to obtain this is the reference cross section, σ_e, in Equation (2.78). It is important to note that in a more general case, where scattering occurs more frequently, the expression in Equation (4.1) describes the number of times a particle is expected to interact with the solar medium throughout the trajectory. Therefore it is only accurate to call it scattering probability in the region where multiple scattering events are highly unlikely.

For the case of a heavy mediator calculating this probability is rather straightforward and multiple scatterings can be neglected if it is significantly smaller than one. In the case of a light mediator, the situation is a bit more intricate. Due to the factor of $\frac{1}{Q^4}$ in the expression, the scattering rate in Equation (2.78) becomes huge for small energy transfers, since small momentum transfers are allowed there from the kinetic requirement. This leads to very large scattering rates almost regardless of the value of the reference cross section, σ_e. To deal with this problem we will, similarly to how they proceeded in Ref. [52], introduce a cutoff parameter, ξ, that ensures that the lowest allowed momentum transfer is

$$Q_{\min} = \xi m_\chi v_\chi. \tag{4.19}$$

This cutoff will come into play when the energy is low enough to bring the bounds on allowed momentum transfers, coming from the kinetic requirements, close to zero.

In Table 4.1 the scattering probabilities calculated as described above are shown. For realistic values, the scattering rates used in the calculations are the ones taking into account the ions in the medium since, as seen in Figures 2.4 and 2.5, the interaction rate can be significantly affected by this, at least around zero transferred energy. Notice that the probabilities are well below one for all of these cases and therefore the assumptions of at most single scattering in the Sun should be reasonable.

Table 4.1: Scattering probabilities in typical trajectories through the Sun for different dark matter masses, and for both heavy and light mediators.

Light mediator		**Heavy mediator**	
$\sigma_e = 10^{-39}$ cm^2, $\xi = 5$		$\sigma_e = 10^{-38}$ cm^2	
MeV	P	MeV	P
0.01	0.2	0.01	0.04
0.1	0.002	0.1	0.2

4.3 Calculations of the Energy Spectra of Reflected Dark Matter Particles

Given the trajectory calculated from the initial velocity and impact parameter, the integral in Equation (4.1) can be performed. In the case of a heavy mediator, the unscreened scattering rate, assuming much larger transferred energies compared to incoming kinetic energies of the dark matter particles, is given in Ref. [52] and looks like

$$\left.\frac{d\Gamma}{d\omega}\right|_{\text{unscreened}} = \frac{\sigma_e n_e}{\sqrt{2\pi m_e T}} \frac{(m_e + m_\chi)^2}{m_e m_\chi} \exp\left(-\frac{\omega}{T}\frac{(m_e + m_\chi)^2}{4 m_e m_\chi}\right). \tag{4.20}$$

By comparing the results from using the unscreened scattering rate and the screened scattering rate given in Equation (2.78), the effect of the medium that was obtained through linear response theory can be investigated.

For the case of the heavy mediator, the comparisons between the unscreened and screened reflection distributions, calculated using Equation (4.2), are shown in Figure 4.2. The dark matter masses used were set to 0.01 MeV and 0.1 MeV, respectively, and the reference cross section, $\bar{\sigma}_e$, is set to 10^{-38} cm^2.

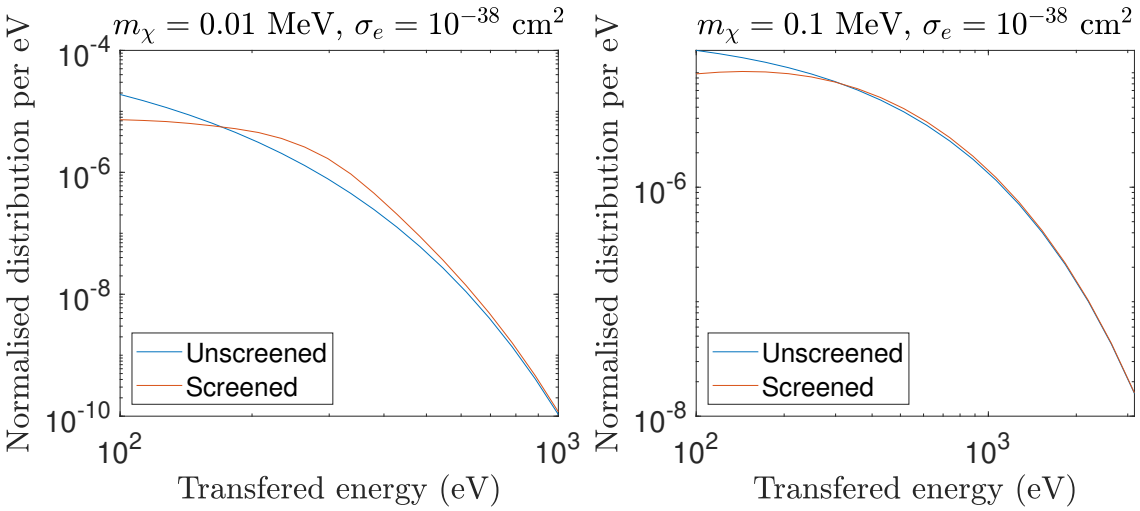

Figure 4.2: Comparison between the screened and unscreened reflected dark matter spectrum in the heavy mediator limit.

Note in Figure 4.2 how the in-medium effects are most important for the lower range of transferred energy, which is reasonable if one compares it to Figure 2.2. Furthermore, one should observe that the discrepancy between the case of included in-medium effect and no in-medium effect is more prominent for the lower mass, which is also to be expected.

As mentioned when discussing the scattering rate in the light mediator limit, the unscreened case is not relevant since the screening is needed to compensate for the extra factor of $\frac{1}{Q^4}$. Therefore, in analogy to the comparisons made in the plots in Figure 2.3, the comparison for the reflection distribution is between the two different expressions for screening using Equation (2.57) and (2.66) respectively in Equation (2.58). The approximated version adapted into the formalism used in this thesis is the version used to account for the medium in Ref. [52]. The comparisons are shown in Figure 4.3 where one should note that the main difference between the two curves is for the lower range of transferred energy, which also agrees with the situations displayed in Figure 2.3. The reference cross section was set to 10^{-39} cm^2 and the cutoff parameter ξ is set to 5, similarly to how they did in Ref. [52] to avoid too small momentum transfers as discussed in Section 4.2.

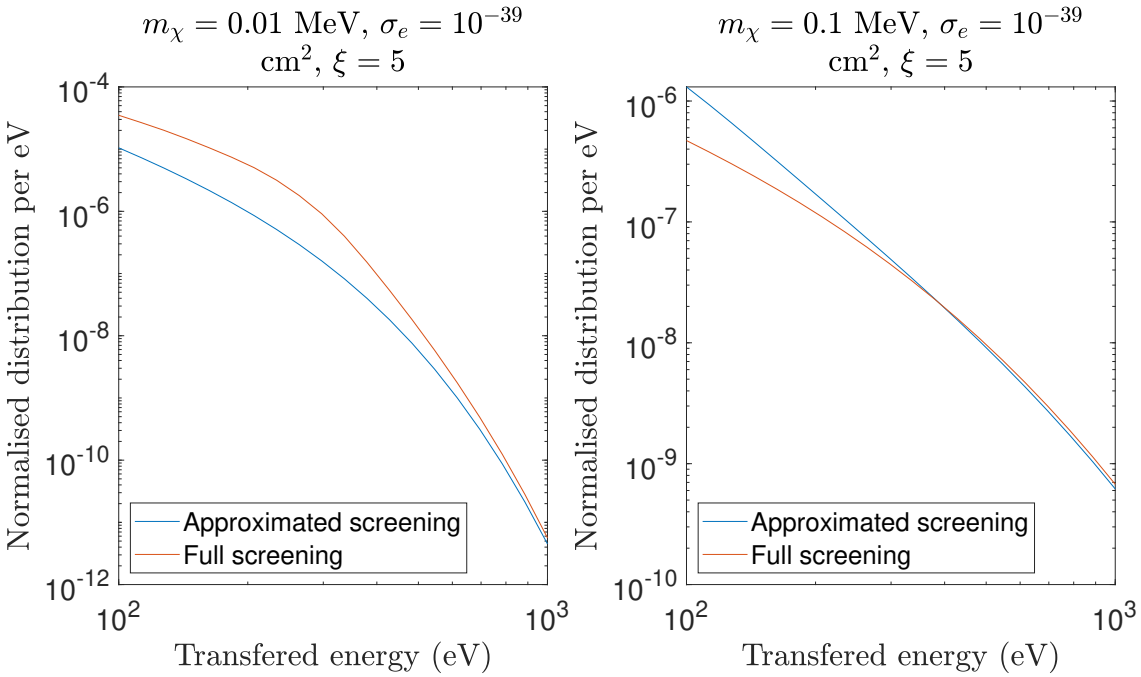

Figure 4.3: Comparison between the screened and unscreened reflected dark matter spectrum in the light mediator limit.

Note in Figure 4.3 how the discrepancy is most noticeable for the lower mass. Another thing to notice in Figure 4.3 is that the rate of reflection is some order of magnitude higher for the lighter dark matter mass. When comparing to Figure 2.3 this is an expected feature, probably caused by the kinetic requirement allowing for lower transferred momenta for the lighter particle.

An important difference between the light and heavy mediator case is the fact that

for the heavy mediator, the distribution of the reflected particles is harder, meaning that there are more particles reflected that have undergone an interaction with higher transferred energy, compared to the much softer reflection distribution for the light mediator case. This preference for softer scattering events for the light mediator should come from the factor of $\frac{1}{Q^4}$, however, due to the cutoff parameter some theoretically allowed interactions are not taken into account. As they argued in Ref. [52] the results should still be reasonable since only interactions containing really small momentum transfers are ignored and those should not significantly impact the spectrum. This should be especially true for the energy regime displayed in Figure 4.3, which is also the regime that is most interesting for solar reflection since that is the regime where the dark matter gets significantly more energetic.

As a final remark on this topic, it is important to remember that all calculations of reflection rates performed in this chapter assumed single scattering. To also investigate scenarios where multiple scatterings are more likely to occur, simulations would have to be conducted which is something that has not been done in this work. However, as demonstrated in Figures 4.2 and 4.3, it could be relevant to, in such simulations, include the in-medium effects as described in this thesis.

5

Conclusion

In this thesis, we have covered how the solar medium affects the interactions between dark matter particles and the electrons in the Sun through the framework of linear response theory. These in-medium effects have both been calculated when only the electrons of the medium were taken into account and when the ions of the medium were included. In terms of the calculated scattering rates, we have demonstrated how they compare to the unscreened scenario in the heavy mediator limit. Similarly, in the light mediator limit, we compared two different types of screenings when calculating the scattering rate, where one used an approximation assuming small momentum and energy transfers. The perhaps most important takeaway from these comparisons was that the largest discrepancies between the unscreened and screened case and between the two models occurred around small transferred energies while, for larger energy transfers, the differences were not as prominent. Another important feature that was hinted at was that the in-medium effect seems most prominent for masses around or below the MeV level.

Before moving on from the topic of scattering rates, the inclusion of ions in the in-medium effect was treated. The result of this showed that the inclusion of ions could help increase the scattering rate quite significantly in the region of small transferred energies. This increased scattering rate was especially prominent in the light mediator limit where it could increase the scattering rate by several orders of magnitude, while in the heavy mediator limit it only increased the scattering rate by about one order of magnitude. In both limits, however, it was clear that the inclusion of ions only appeared to have a significant effect on the scattering rate in the region of small transferred energies, while the effect of the ions almost disappeared in the regions of larger transferred energies.

After having treated these scattering rates we used the derived expressions to calculate the rate at which dark matter particles could interact in such a way that they become gravitationally bound to the Sun. As pointed out, in connection to these calculations the rate at which dark matter particles could get captured is far lower compared to the rate at which they instead could get accelerated, i.e. reflected, by the Sun due to the rather small phase space available for capture. Furthermore, it was pointed out how the scenario of dark matter particles undergoing several interactions where it initially might get gravitationally bound before being accelerated

into unbound energies again might be an interesting subject to investigate via simulations, something that was not done in this thesis. Still, the rate at which dark matter particles could undergo scatterings where they become gravitationally bound was calculated in both the light and heavy mediator limit for various dark matter masses and reference cross sections. In the heavy mediator case, one could notice how the rate of capture was directly linked to the size of the available phase space or equivalently the mass of the dark matter particle. However, in the light mediator limit, it was noted how, in fact, the lighter masses, where the available phase space is smaller, had a higher capture rate. The presumed reason for this, perhaps an unexpected feature, was discussed and the presented hypothesis was that the kinematic requirement allowing for smaller transferred momenta for smaller masses in combination with the factor of $\frac{1}{Q^4}$ was the cause.

The final subject brought up in the thesis was the topic of dark matter reflections. As hinted upon when discussing dark matter capture, this might be a more promising avenue to investigate for the rather low range of dark matter masses treated in this thesis, since here there is no problem with a small available phase space. In analogy to when the scattering rates were discussed earlier, here the expected reflected spectra were compared between the unscreened and screened case in the heavy mediator limit and in the light mediator limit, the comparison was between the two different versions of screening. The result of the comparisons showed that the screening could be of importance, especially towards the region of slightly lower transferred energies.

Further topics that might be of interest for future works could be to implement the in-medium effect, as presented in this thesis, in simulations of solar dark matter interactions like, perhaps most importantly, dark matter reflections. This thesis only assumed single scattering scenarios where the reflection could be treated analytically, and since some discrepancies could be demonstrated compared to the unscreened case, or the other version of screening, simulations using the scattering rates presented in this thesis could be of interest.

In conclusion, we have, in this thesis, shown that the in-medium effect, calculated using linear response theory, could be of some importance, especially for dark matter masses below the MeV level. Furthermore, we have demonstrated how these in-medium effects could affect the, for this mass range, perhaps most important topic of solar dark matter reflection, as well as applying it to the phenomenon of dark matter capture.

Bibliography

[1] G. Bertone and D. Hooper, "History of dark matter," *Reviews of Modern Physics*, vol. 90, no. 4, Oct. 2018, ISSN: 1539-0756. DOI: 10.1103/revmodphys.90.045002. [Online]. Available: http://dx.doi.org/10.1103/RevModPhys.90.045002.

[2] J. Einasto, *Dark matter*, 2010. arXiv: 0901.0632 [astro-ph.CO].

[3] H. Andernach and F. Zwicky, *English and spanish translation of zwicky's (1933) the redshift of extragalactic nebulae*, 2017. arXiv: 1711.01693 [astro-ph.IM].

[4] V. C. Rubin, W. K. Ford Jr., and N. Thonnard, "Extended rotation curves of high-luminosity spiral galaxies. IV. Systematic dynamical properties, Sa through Sc," *Astrophys. J. Lett.*, vol. 225, pp. L107–L111, 1978. DOI: 10.1086/182804.

[5] M. S. Roberts and A. H. Rots, "Comparison of Rotation Curves of Different Galaxy Types," *Astronomy and Astrophysics*, vol. 26, pp. 483–485, Aug. 1973.

[6] A. Bosma, "The distribution and kinematics of neutral hydrogen in spiral galaxies of various morphological types," Ph.D. dissertation, University of Groningen, Netherlands, Mar. 1978.

[7] J. P. Ostriker, P. J. E. Peebles, and A. Yahil, "The Size and Mass of Galaxies, and the Mass of the Universe," *Astrophysical Journal*, vol. 193, p. L1, Oct. 1974. DOI: 10.1086/181617.

[8] J. Einasto, E. Saar, A. Kaasik, and A. D. Chernin, "Missing mass around galaxies - Morphological evidence," *Nature*, vol. 252, pp. 111–113, Nov. 1974. DOI: 10.1038/252111a0.

[9] J. Einasto, A. Kaasik, and E. Saar, "Dynamic evidence on massive coronas of galaxies," *Nature*, vol. 250, no. 5464, pp. 309–310, Jul. 1974. DOI: 10.1038/250309a0.

[10] E. Komatsu *et al.*, "Five-Year Wilkinson Microwave Anisotropy Probe Observations: Cosmological Interpretation," *The Astrophysical Journal Supplement*, vol. 180, no. 2, pp. 330–376, Feb. 2009. DOI: 10.1088/0067-0049/180/2/330. arXiv: 0803.0547 [astro-ph].

[11] E. Komatsu *et al.*, "Seven-year Wilkinson Microwave Anisotropy Probe (WMAP) Observations: Cosmological Interpretation," *The Astrophysical Journal Supplement*, vol. 192, no. 2, 18, p. 18, Feb. 2011. DOI: 10.1088/0067-0049/192/2/18. arXiv: 1001.4538 [astro-ph.CO].

[12] P. A. R. Ade *et al.*, "Planck2015 results: Xiii. cosmological parameters," *Astronomy and Astrophysics*, vol. 594, A13, Sep. 2016, ISSN: 1432-0746. DOI:

10.1051/0004-6361/201525830. [Online]. Available: http://dx.doi.org/10.1051/0004-6361/201525830.

[13] A. L. Coil, "The large-scale structure of the universe," in *Planets, Stars and Stellar Systems*. Springer Netherlands, 2013, pp. 387–421. DOI: 10.1007/978-94-007-5609-0_8. [Online]. Available: http://dx.doi.org/10.1007/978-94-007-5609-0_8.

[14] R. Massey, T. Kitching, and J. Richard, "The dark matter of gravitational lensing," *Reports on Progress in Physics*, vol. 73, no. 8, p. 086 901, Jul. 2010, ISSN: 1361-6633. DOI: 10.1088/0034-4885/73/8/086901. [Online]. Available: http://dx.doi.org/10.1088/0034-4885/73/8/086901.

[15] M. Bradač *et al.*, "Revealing the properties of dark matter in the merging cluster macs j0025.41222," *The Astrophysical Journal*, vol. 687, no. 2, pp. 959–967, Nov. 2008, ISSN: 1538-4357. DOI: 10.1086/591246. [Online]. Available: http://dx.doi.org/10.1086/591246.

[16] G. Steigman and M. S. Turner, "Cosmological Constraints on the Properties of Weakly Interacting Massive Particles," *Nucl. Phys. B*, vol. 253, pp. 375–386, 1985. DOI: 10.1016/0550-3213(85)90537-1.

[17] P. Gondolo and G. Gelmini, "Cosmic abundances of stable particles: Improved analysis," *Nuclear Physics B*, vol. 360, no. 1, pp. 145–179, 1991, ISSN: 0550-3213. DOI: https://doi.org/10.1016/0550-3213(91)90438-4. [Online]. Available: https://www.sciencedirect.com/science/article/pii/0550321391904384.

[18] K. Griest and D. Seckel, "Three exceptions in the calculation of relic abundances," *Phys. Rev. D*, vol. 43, pp. 3191–3203, 10 May 1991. DOI: 10.1103/PhysRevD.43.3191. [Online]. Available: https://link.aps.org/doi/10.1103/PhysRevD.43.3191.

[19] M. Srednicki, R. Watkins, and K. A. Olive, "Calculations of relic densities in the early universe," *Nuclear Physics B*, vol. 310, no. 3, pp. 693–713, 1988, ISSN: 0550-3213. DOI: https://doi.org/10.1016/0550-3213(88)90099-5. [Online]. Available: https://www.sciencedirect.com/science/article/pii/0550321388900995.

[20] J. L. Feng, "Naturalness and the status of supersymmetry," *Annual Review of Nuclear and Particle Science*, vol. 63, no. 1, pp. 351–382, Oct. 2013, ISSN: 1545-4134. DOI: 10.1146/annurev-nucl-102010-130447. [Online]. Available: http://dx.doi.org/10.1146/annurev-nucl-102010-130447.

[21] R. D. Peccei and H. R. Quinn, "Constraints imposed by CP conservation in the presence of pseudoparticles," *Phys. Rev. D*, vol. 16, pp. 1791–1797, 6 Sep. 1977. DOI: 10.1103/PhysRevD.16.1791. [Online]. Available: https://link.aps.org/doi/10.1103/PhysRevD.16.1791.

[22] R. D. Peccei and H. R. Quinn, "CP Conservation in the presence of pseudoparticles," *Phys. Rev. Lett.*, vol. 38, pp. 1440–1443, 25 Jun. 1977. DOI: 10.1103/PhysRevLett.38.1440. [Online]. Available: https://link.aps.org/doi/10.1103/PhysRevLett.38.1440.

[23] F. Wilczek, "Problem of strong P and T invariance in the presence of instantons," *Phys. Rev. Lett.*, vol. 40, pp. 279–282, 5 Jan. 1978. DOI: 10.1103/

PhysRevLett.40.279. [Online]. Available: https://link.aps.org/doi/10.1103/PhysRevLett.40.279.

[24] S. Weinberg, "A new light boson?" *Phys. Rev. Lett.*, vol. 40, pp. 223–226, 4 Jan. 1978. DOI: 10.1103/PhysRevLett.40.223. [Online]. Available: https://link.aps.org/doi/10.1103/PhysRevLett.40.223.

[25] M. Dine, W. Fischler, and M. Srednicki, "A simple solution to the strong cp problem with a harmless axion," *Physics Letters B*, vol. 104, no. 3, pp. 199–202, 1981, ISSN: 0370-2693. DOI: https://doi.org/10.1016/0370-2693(81)90590-6. [Online]. Available: https://www.sciencedirect.com/science/article/pii/0370269381905906.

[26] J. E. Kim, "Weak-interaction singlet and strong CP invariance," *Phys. Rev. Lett.*, vol. 43, pp. 103–107, 2 Jul. 1979. DOI: 10.1103/PhysRevLett.43.103. [Online]. Available: https://link.aps.org/doi/10.1103/PhysRevLett.43.103.

[27] M. Shifman, A. Vainshtein, and V. Zakharov, "Can confinement ensure natural cp invariance of strong interactions?" *Nuclear Physics B*, vol. 166, no. 3, pp. 493–506, 1980, ISSN: 0550-3213. DOI: https://doi.org/10.1016/0550-3213(80)90209-6. [Online]. Available: https://www.sciencedirect.com/science/article/pii/0550321380902096.

[28] T. W. Kephart and T. J. Weiler, "Luminous axion clusters," *Phys. Rev. Lett.*, vol. 58, pp. 171–173, 2 Jan. 1987. DOI: 10.1103/PhysRevLett.58.171. [Online]. Available: https://link.aps.org/doi/10.1103/PhysRevLett.58.171.

[29] M. S. Turner, "Early-universe thermal production of not-so-invisible axions," *Phys. Rev. Lett.*, vol. 59, pp. 2489–2492, 21 Nov. 1987. DOI: 10.1103/PhysRevLett.59.2489. [Online]. Available: https://link.aps.org/doi/10.1103/PhysRevLett.59.2489.

[30] L. Abbott and P. Sikivie, "A cosmological bound on the invisible axion," *Physics Letters B*, vol. 120, no. 1, pp. 133–136, 1983, ISSN: 0370-2693. DOI: https://doi.org/10.1016/0370-2693(83)90638-X. [Online]. Available: https://www.sciencedirect.com/science/article/pii/037026938390638X.

[31] M. Dine and W. Fischler, "The not-so-harmless axion," *Physics Letters B*, vol. 120, no. 1, pp. 137–141, 1983, ISSN: 0370-2693. DOI: https://doi.org/10.1016/0370-2693(83)90639-1. [Online]. Available: https://www.sciencedirect.com/science/article/pii/0370269383906391.

[32] J. Preskill, M. B. Wise, and F. Wilczek, "Cosmology of the invisible axion," *Physics Letters B*, vol. 120, no. 1, pp. 127–132, 1983, ISSN: 0370-2693. DOI: https://doi.org/10.1016/0370-2693(83)90637-8. [Online]. Available: https://www.sciencedirect.com/science/article/pii/0370269383906378.

[33] A. Boyarsky, M. Drewes, T. Lasserre, S. Mertens, and O. Ruchayskiy, "Sterile neutrino dark matter," *Progress in Particle and Nuclear Physics*, vol. 104, pp. 1–45, Jan. 2019, ISSN: 0146-6410. DOI: 10.1016/j.ppnp.2018.07.004. [Online]. Available: http://dx.doi.org/10.1016/j.ppnp.2018.07.004.

[34] J. H. MacGibbon, "Can Planck-mass relics of evaporating black holes close the universe?" *Nature*, vol. 329, pp. 308–309, 1987. DOI: 10.1038/329308a0.

[35] H. I. Kim, C. H. Lee, and J. H. MacGibbon, "Diffuse γ-ray background and primordial black hole constraints on the spectral index of density fluctuations," *Phys. Rev. D*, vol. 59, p. 063 004, 6 Feb. 1999. DOI: 10.1103/PhysRevD.59.063004. [Online]. Available: https://link.aps.org/doi/10.1103/PhysRevD.59.063004.

[36] J. Yokoyama, "Cosmological constraints on primordial black holes produced in the near-critical gravitational collapse," *Phys. Rev. D*, vol. 58, p. 107 502, 10 Oct. 1998. DOI: 10.1103/PhysRevD.58.107502. [Online]. Available: https://link.aps.org/doi/10.1103/PhysRevD.58.107502.

[37] M. Milgrom, "A modification of the Newtonian dynamics as a possible alternative to the hidden mass hypothesis.," *Astrophysical Journal*, vol. 270, pp. 365–370, Jul. 1983. DOI: 10.1086/161130.

[38] M. Milgrom, "A modification of the Newtonian dynamics - Implications for galaxies.," *Astrophysical Journal*, vol. 270, pp. 371–383, Jul. 1983. DOI: 10.1086/161131.

[39] M. Milgrom, "A modification of the newtonian dynamics : implications for galaxy systems.," *Astrophysical Journal*, vol. 270, pp. 384–389, Jul. 1983. DOI: 10.1086/161132.

[40] J. Bekenstein, "Relativistic gravitation theory for the modified newtonian dynamics paradigm," *Phys. Rev. D*, vol. 70, Oct. 2004. DOI: 10.1103/PhysRevD.70.083509.

[41] A. Goudelis, "Dark matter at the LHC: WIMPs and beyond," *PoS*, vol. LHCP2019, p. 187, 2019. DOI: 10.22323/1.350.0187.

[42] G. Bertone, "The moment of truth for wimp dark matter," *Nature*, vol. 468, no. 7322, pp. 389–393, Nov. 2010, ISSN: 1476-4687. DOI: 10.1038/nature09509. [Online]. Available: http://dx.doi.org/10.1038/nature09509.

[43] J. Silk and M. Srednicki, "Cosmic-ray antiprotons as a probe of a photino-dominated universe," *Phys. Rev. Lett.*, vol. 53, pp. 624–627, 6 Aug. 1984. DOI: 10.1103/PhysRevLett.53.624. [Online]. Available: https://link.aps.org/doi/10.1103/PhysRevLett.53.624.

[44] L. M. Krauss, K. Freese, D. N. Spergel, and W. H. Press, "Cold dark matter candidates and the solar neutrino problem," *Astrophysical Journal*, vol. 299, pp. 1001–1006, Dec. 1985. DOI: 10.1086/163767.

[45] Z.-L. Liang and P. Zhang, "The linear response theory approach to the sub-gev dark matter in the sun," *Journal of Cosmology and Astroparticle Physics*, vol. 2023, no. 12, p. 009, Dec. 2023. DOI: 10.1088/1475-7516/2023/12/009. [Online]. Available: https://dx.doi.org/10.1088/1475-7516/2023/12/009.

[46] L. Barak *et al.*, "Sensei: Direct-detection results on sub-gev dark matter from a new skipper ccd," *Phys. Rev. Lett.*, vol. 125, p. 171 802, 17 Oct. 2020. DOI: 10.1103/PhysRevLett.125.171802. [Online]. Available: https://link.aps.org/doi/10.1103/PhysRevLett.125.171802.

[47] N. Castelló-Mor, "Damic-m experiment: Thick, silicon ccds to search for light dark matter," *Nuclear Instruments and Methods in Physics Research Section A: Accelerators, Spectrometers, Detectors and Associated Equipment*, vol. 958, p. 162 933, 2020, Proceedings of the Vienna Conference on Instrumentation

2019, ISSN: 0168-9002. DOI: https://doi.org/10.1016/j.nima.2019.162933. [Online]. Available: https://www.sciencedirect.com/science/article/pii/S0168900219313336.

[48] D. W. Amaral *et al.*, "Constraints on low-mass, relic dark matter candidates from a surface-operated supercdms single-charge sensitive detector," *Phys. Rev. D*, vol. 102, p. 091 101, 9 Nov. 2020. DOI: 10.1103/PhysRevD.102.091101. [Online]. Available: https://link.aps.org/doi/10.1103/PhysRevD.102.091101.

[49] Z. Y. Zhang *et al.*, "Constraints on sub-gev dark matter–electron scattering from the cdex-10 experiment," *Phys. Rev. Lett.*, vol. 129, p. 221 301, 22 Nov. 2022. DOI: 10.1103/PhysRevLett.129.221301. [Online]. Available: https://link.aps.org/doi/10.1103/PhysRevLett.129.221301.

[50] Q. Arnaud *et al.*, "First germanium-based constraints on sub-mev dark matter with the edelweiss experiment," *Phys. Rev. Lett.*, vol. 125, p. 141 301, 14 Oct. 2020. DOI: 10.1103/PhysRevLett.125.141301. [Online]. Available: https://link.aps.org/doi/10.1103/PhysRevLett.125.141301.

[51] W. DeRocco, M. Galanis, and R. Lasenby, "Dark matter scattering in astrophysical media: Collective effects," *Journal of Cosmology and Astroparticle Physics*, vol. 2022, no. 05, p. 015, May 2022, ISSN: 1475-7516. DOI: 10.1088/1475-7516/2022/05/015. [Online]. Available: http://dx.doi.org/10.1088/1475-7516/2022/05/015.

[52] H. An, H. Nie, M. Pospelov, J. Pradler, and A. Ritz, "Solar reflection of dark matter," *Physical Review D*, vol. 104, no. 10, Nov. 2021, ISSN: 2470-0029. DOI: 10.1103/physrevd.104.103026. [Online]. Available: http://dx.doi.org/10.1103/PhysRevD.104.103026.

[53] A. Mitridate, T. Trickle, Z. Zhang, and K. M. Zurek, "Dark matter absorption via electronic excitations," *Journal of High Energy Physics*, vol. 2021, no. 9, Sep. 2021, ISSN: 1029-8479. DOI: 10.1007/jhep09(2021)123. [Online]. Available: http://dx.doi.org/10.1007/JHEP09(2021)123.

[54] T. Emken, "Solar reflection of light dark matter with heavy mediators," *Physical Review D*, vol. 105, no. 6, Mar. 2022, ISSN: 2470-0029. DOI: 10.1103/physrevd.105.063020. [Online]. Available: http://dx.doi.org/10.1103/PhysRevD.105.063020.

[55] T. Emken, R. Essig, and H. Xu, "Solar reflection of dark matter with dark-photon mediators," Apr. 2024. arXiv: 2404.10066 [hep-ph].

[56] T. M. Inc., *Matlab version: R2021a*, Natick, Massachusetts, United States, 2021. [Online]. Available: https://www.mathworks.com.

[57] J. Sólyom, *Fundamentals of the Physics of Solids: Volume 3 - Normal, Broken-Symmetry, and Correlated Systems*. Springer Berlin, 2010, vol. 3. DOI: https://doi.org/10.1007/978-3-642-04518-9.

[58] J. N. Bahcall and R. K. Ulrich, "Solar models, neutrino experiments, and helioseismology," *Rev. Mod. Phys.*, vol. 60, pp. 297–372, 2 Apr. 1988. DOI: 10.1103/RevModPhys.60.297. [Online]. Available: https://link.aps.org/doi/10.1103/RevModPhys.60.297.

A

Linear Response Theory

This appendix follows Ref. [57], especially appendix J, quite closely and aims to give an introduction to the field of linear response theory to understand its implementation in this thesis.

To begin with, consider a system with time-independent Hamiltonian H_0 and energy eigenstates $|\psi_n\rangle$ with corresponding eigenenergies E_n. Assume now that this system is perturbed by a weak external Hamiltonian that generally can be written on the form

$$H_{\text{ext}}(t) = -\int d\mathbf{x} B(\mathbf{x}) F(\mathbf{x}, t) \tag{A.1}$$

where B is some operator and F is the strength of the perturbation.

Assume now that $F(\mathbf{r}, t) = F(t) = F_0\delta(t)$, meaning a spatially uniform perturbation at $t = 0$. If F_0 is small the change in the observable A can be written as

$$\langle \Delta A(t) \rangle = \chi_{AB}(t) F_0 \tag{A.2}$$

where χ_{AB} is the so-called response function that for physical reasons has to vanish for $t < 0$ since then the perturbation has not yet taken place. When the perturbation changes in time it can be expressed as

$$F(t) = \int_{-\infty}^{\infty} F(t')\delta(t - t')dt' \tag{A.3}$$

and the effect on the observable A can be expressed as

$$\langle \Delta A(t) \rangle = \int_{-\infty}^{t} dt' \chi_{AB}(t - t') F(t') = \int_{0}^{\infty} dt' \chi_{AB}(t') F(t - t'). \tag{A.4}$$

If the external perturbation also has a spatial dependence, the now spatially dependent response function can be defined via the relation

$$\langle \Delta A(\mathbf{x}, t) \rangle = \int_{0}^{\infty} dt' \int d\mathbf{x}' \chi_{AB}(\mathbf{x}, \mathbf{x}', t') F(\mathbf{x}', t - t'). \tag{A.5}$$

Assuming that the unperturbed system is spatially uniform, the response can only depend on the difference between $\mathbf{x}$ and $\mathbf{x}'$ leading to

$$\langle \Delta A(\mathbf{x},t)\rangle = \int_0^\infty dt' \int d\mathbf{x}' \chi_{AB}(\mathbf{x}-\mathbf{x}',t')F(\mathbf{x}',t-t'). \tag{A.6}$$

Taking the Fourier transform with respect to the spatial variable leads to

$$\begin{aligned} \langle \Delta A(\mathbf{Q},t)\rangle = \int d\mathbf{x}\langle \Delta A(\mathbf{x},t)\rangle e^{i\mathbf{x}\cdot\mathbf{Q}} = \\ \int d\mathbf{x}\int_0^\infty dt' \int d\mathbf{x}' \chi_{AB}(\mathbf{x}-\mathbf{x}',t')F(\mathbf{x}',t-t')e^{i\mathbf{x}\cdot\mathbf{Q}} = \\ \int d\mathbf{x}\int_0^\infty dt' \int d\mathbf{x}' \chi_{AB}(\mathbf{x}-\mathbf{x}',t')e^{i(\mathbf{x}-\mathbf{x}')\cdot\mathbf{Q}}F(\mathbf{x}',t-t')e^{i\mathbf{x}'\cdot\mathbf{Q}} = \\ \int_0^\infty dt' \chi_{AB}(\mathbf{Q},t')F(\mathbf{Q},t-t'). \end{aligned} \tag{A.7}$$

By also taking the Fourier transform to the frequency domain, the now momentum and energy-dependent response becomes

$$\langle \Delta A(\mathbf{Q},\omega)\rangle = \chi_{AB}(\mathbf{Q},\omega)F(\mathbf{Q},\omega). \tag{A.8}$$

Since the response function vanishes for negative time arguments, its Fourier transform can be written

$$\chi_{AB}(\mathbf{Q},\omega) = \int_0^\infty \chi_{AB}(\mathbf{Q},t)e^{i\omega t}dt. \tag{A.9}$$

Because the response to a real perturbation has to be real, the response function $\chi_{AB}(\mathbf{Q},\omega)$ has to satisfy the relation

$$\chi_{AB}(\mathbf{Q},\omega) = \chi^*_{AB}(\mathbf{Q},-\omega) \tag{A.10}$$

which means that, when decomposed into real and imaginary parts according to

$$\chi_{AB}(\mathbf{Q},\omega) = \mathrm{Re}(\chi_{AB}(\mathbf{Q},\omega)) + i\mathrm{Im}(\chi_{AB}(\mathbf{Q},\omega)), \tag{A.11}$$

the real part is an even function of frequency while the imaginary part is an odd function of frequency

$$\mathrm{Re}(\chi_{AB}(\mathbf{Q},\omega)) = \mathrm{Re}(\chi_{AB}(\mathbf{Q},-\omega)) \tag{A.12}$$

$$\mathrm{Im}(\chi_{AB}(\mathbf{Q},\omega)) = -\mathrm{Im}(\chi_{AB}(\mathbf{Q},-\omega)). \tag{A.13}$$

Moving on to looking more at what the expectation value of the observable A in the perturbed system is, it can be described in terms of the density matrix, $\rho(t)$, of the perturbed system through the relation

$$\langle A\rangle = \mathrm{Tr}(\rho A) \tag{A.14}$$

where the density matrix can be calculated from its Equation of motion, given by

$$\frac{d\rho(t)}{dt} = i[\rho(t), H_0 + H_{\mathrm{ext}}(t)]. \tag{A.15}$$

This Equation can be solved by making use of the interaction picture where

$$\begin{aligned}\frac{d}{dt}(e^{iH_0t}\rho(t)e^{iH_0t}e^{-iH_0t}) = \\ iH_0e^{iH_0t}\rho(t)e^{-iH_0t} - ie^{iH_0t}\rho(t)H_0e^{-iH_0t} + ie^{iH_0t}[\rho(t), H_0 + H_{\text{ext}}(t)]e^{-iH_0t} = \\ ie^{iH_0t}\left([H_0, \rho(t)] + [\rho(t), H_0 + H_{\text{ext}}(t)]\right)e^{-iH_0t} = ie^{iH_0t}[\rho(t), H_{\text{ext}}(t)]e^{-iH_0t},\end{aligned} \tag{A.16}$$

and by integrating this Equation with the boundary condition that $\rho(t \to -\infty) = \rho_0$, where ρ_0 is the density matrix of the unperturbed system, the Equation for the density matrix becomes

$$\begin{aligned}e^{iH_0t}\rho(t)e^{iH_0t}e^{-iH_0t} &= \rho_0 + i\int_{-\infty}^{t} e^{iH_0t'}[\rho(t'), H_{\text{ext}}(t')]e^{-iH_0t'}dt' \\ \iff \rho(t) &= \rho_0 + i\int_{-\infty}^{t} e^{-iH_0(t-t')}[\rho(t'), H_{\text{ext}}(t')]e^{iH_0(t-t')}dt'.\end{aligned} \tag{A.17}$$

By solving this Equation iteratively, i.e. putting the full expression for $\rho(t)$ into $\rho(t')$ in the right-hand side, going to at most first order in the perturbation, the density matrix can be expressed

$$\rho(t) = \rho_0 + i\int_{-\infty}^{t} e^{-iH_0(t-t')}[\rho_0, H_{\text{ext}}(t')]e^{iH_0(t-t')}dt'. \tag{A.18}$$

To now obtain $\langle \Delta A(\mathbf{x}, t)\rangle$ it is first important to observe that $\langle A\rangle = \text{Tr}(\rho A) = \text{Tr}(\rho_0 A) + \langle \Delta A(\mathbf{x}, t)\rangle$ which implies that

$$\langle \Delta A(\mathbf{x}, t)\rangle = i\int_{-\infty}^{t} \text{Tr}\left(e^{-iH_0(t-t')}[\rho_0, H_{\text{ext}}(t')]e^{iH_0(t-t')}A(\mathbf{x})\right)dt', \tag{A.19}$$

and by using the cyclic property of the trace and the interaction picture formulation this expression can be rewritten

$$\begin{aligned}\langle \Delta A(\mathbf{x}, t)\rangle = i\int_{-\infty}^{t} \text{Tr}\left(e^{iH_0(t-t')}A(\mathbf{x})e^{-iH_0(t-t')}[\rho_0, H_{\text{ext}}(t')]\right)dt' = \\ i\int_{-\infty}^{t} \text{Tr}\left(A(\mathbf{x}, t-t')(\rho_0 H_{\text{ext}}(t') - H_{\text{ext}}(t')\rho_0)\right)dt' = \\ i\int_{-\infty}^{t} \text{Tr}\left(\rho_0(H_{\text{ext}}(t')A(\mathbf{x}, t-t') - H_{\text{ext}}(t')A(\mathbf{x}, t-t'))\right)dt' = \\ -i\int_{-\infty}^{t} \text{Tr}\left(\rho_0[A(\mathbf{x}, t-t'), H_{\text{ext}}(t')]\right)dt'.\end{aligned} \tag{A.20}$$

With the perturbation Hamiltonian given in Equation (A.1), the expectation value for the change in the observable A can be written as

$$\langle \Delta A(\mathbf{x}, t)\rangle = -i\int_{-\infty}^{t} \text{Tr}\left(\rho_0\left[A(\mathbf{x}, t-t'), -\int d\mathbf{x}' B(\mathbf{x}')F(\mathbf{x}', t')\right]\right)dt', \tag{A.21}$$

and since F is just the strength of the perturbation and not an operator

$$\begin{aligned}\langle \Delta A(\mathbf{x},t)\rangle = i\int_{-\infty}^{t} \mathrm{Tr}\left(\rho_0\left[A(\mathbf{x},t-t'),\int d\mathbf{x}' B(\mathbf{x}')\right]\right)F(\mathbf{x}',t')dt' = \\ i\int_{-\infty}^{t}\int d\mathbf{x}' \mathrm{Tr}\left(\rho_0\left[A(\mathbf{x},t-t'),B(\mathbf{x}')\right]\right)F(\mathbf{x}',t')dt'.\end{aligned} \tag{A.22}$$

Using the definition that $\mathrm{Tr}\left(\rho_0\left[A(\mathbf{x},t-t'),B(\mathbf{x}')\right]\right) = \langle[A(\mathbf{x},t-t'),B(\mathbf{x}')]\rangle$, the above expression can be written

$$\langle \Delta A(\mathbf{x},t)\rangle = i\int_{-\infty}^{t}\int d\mathbf{x}'\langle[A(\mathbf{x},t-t'),B(\mathbf{x}')]\rangle F(\mathbf{x}',t')dt'. \tag{A.23}$$

If this expression for $\langle \Delta A(\mathbf{x},t)\rangle$ is compared to the expression in Equation (A.5), an expression for the response function $\chi_{AB}(\mathbf{x},\mathbf{x}',t-t')$ can be obtained according to

$$\chi_{AB}(\mathbf{x},\mathbf{x}',t-t') = \begin{cases} i\langle[A(\mathbf{x},t-t'),B(\mathbf{x}')]\rangle, & t>t' \\ 0, & t<t' \end{cases}. \tag{A.24}$$

By rearranging the time dependence in the right-hand side of the above expression, using the cyclic property of the trace and the fact that ρ_0 and H_0 commute according to

$$\begin{aligned}\langle[A(\mathbf{x},t-t'),B(\mathbf{x}')]\rangle = \\ \mathrm{Tr}\left(\rho_0\left(e^{iH_0(t-t')}A(\mathbf{x})e^{-iH_0(t-t')}B(\mathbf{x}') - B(\mathbf{x}')e^{iH_0(t-t')}A(\mathbf{x})e^{-iH_0(t-t')}\right)\right) = \\ \mathrm{Tr}\left(\rho_0\left(e^{-iH_0t'}A(\mathbf{x},t)e^{iH_0t'}B(\mathbf{x}') - B(\mathbf{x}')e^{-iH_0t'}A(\mathbf{x},t)e^{iH_0t'}\right)\right) = \\ \mathrm{Tr}\left(A(\mathbf{x},t)e^{iH_0t'}B(\mathbf{x}')\rho_0e^{-iH_0t'} - e^{iH_0t'}\rho_0B(\mathbf{x}')e^{-iH_0t'}A(\mathbf{x},t)\right) = \\ \mathrm{Tr}\left(A(\mathbf{x},t)e^{iH_0t'}B(\mathbf{x}')e^{-iH_0t'}\rho_0 - \rho_0e^{iH_0t'}B(\mathbf{x}')e^{-iH_0t'}A(\mathbf{x},t)\right) = \\ \mathrm{Tr}\left(\rho_0\left(A(\mathbf{x},t)B(\mathbf{x}',t') - B(\mathbf{x}',t')A(\mathbf{x},t)\right)\right) = \langle[A(\mathbf{x},t),B(\mathbf{x}',\mathbf{t}')]\rangle,\end{aligned} \tag{A.25}$$

the expression for the response function, $\chi_{AB}(\mathbf{x},\mathbf{x}',t-t')$, can be rewritten

$$\chi_{AB}(\mathbf{x},\mathbf{x}',t-t') = \begin{cases} i\langle[A(\mathbf{x},t),B(\mathbf{x}',t')]\rangle, & t>t' \\ 0, & t<t' \end{cases} \tag{A.26}$$

or equivalently

$$\chi_{AB}(\mathbf{x},\mathbf{x}',t-t') = i\theta(t-t')\langle[A(\mathbf{x},t),B(\mathbf{x}',t')]\rangle \tag{A.27}$$

where θ is the Heaviside step function. This expression is also known as the Kubo formula. As before, if the system is translation invariant, the response function can only depend on $\mathbf{x}-\mathbf{x}'$ which means that the spatial Fourier transform becomes

$$\begin{aligned}\chi_{AB}(\mathbf{Q},t-t') = i\theta(t-t')\int d(\mathbf{x}-\mathbf{x}')\langle[A(\mathbf{x},t),B(\mathbf{x}',t')]\rangle e^{i\mathbf{Q}\cdot(\mathbf{x}-\mathbf{x}')} = \\ i\theta(t-t')\langle[A(\mathbf{Q},t),B(\mathbf{x}',t')]\rangle e^{-i\mathbf{Q}\cdot\mathbf{x}'} = i\theta(t-t')\frac{1}{V}\int d\mathbf{r}'\langle[A(\mathbf{Q},t),B(\mathbf{x}',t')]\rangle e^{-i\mathbf{Q}\cdot\mathbf{x}'} = \\ i\theta(t-t')\langle[A(\mathbf{Q},t),B(-\mathbf{Q},t')]\rangle.\end{aligned} \tag{A.28}$$

Also taking the Fourier transformation with respect to time leads to

$$\chi_{AB}(\mathbf{Q},\omega) = i\int_0^\infty d(t-t')e^{i\omega(t-t')}\frac{1}{V}\langle[A(\mathbf{Q},t),B(-\mathbf{Q},t')]\rangle. \tag{A.29}$$

Using the fact that the density matrix of the unperturbed system, ρ_0, can be written

$$\rho_0 = \frac{1}{Z}e^{-\beta H_0} \tag{A.30}$$

where Z is the partition function of the system given by $Z=\sum_n e^{-\beta E_n}$, the above expression for the Fourier transformed response function can be rewritten

$$\begin{aligned}\chi_{AB}(\mathbf{Q},\omega) = i\int_0^\infty d(t-t')e^{i\omega(t-t')}\frac{1}{V}\\ \mathrm{Tr}\left(\frac{1}{Z}e^{-\beta H_0}(A(\mathbf{Q},t)B(-\mathbf{Q},t')-B(-\mathbf{Q},t')A(\mathbf{Q},t))\right) =\\ i\int_0^\infty d(t-t')e^{i\omega(t-t')}\frac{1}{V}\sum_n\langle\psi_n|\,\frac{1}{Z}e^{-\beta H_0}(A(\mathbf{Q},t)B(-\mathbf{Q},t')-B(-\mathbf{Q},t')A(\mathbf{Q},t))\,|\psi_n\rangle =\\ i\int_0^\infty d(t-t')e^{i\omega(t-t')}\frac{1}{V}\sum_n\frac{1}{Z}e^{-\beta H_0}\,\langle\psi_n|\,A(\mathbf{Q},t)B(-\mathbf{Q},t')-B(-\mathbf{Q},t')A(\mathbf{Q},t)\,|\psi_n\rangle\,.\end{aligned} \tag{A.31}$$

By now utilising the completeness relation, $\sum_m |\psi_m\rangle\langle\psi_m|=1$, the above expression becomes

$$\begin{aligned}\chi_{AB}(\mathbf{Q},\omega) = i\int_0^\infty d(t-t')e^{i\omega(t-t')}\frac{1}{V}\sum_{mn}\frac{1}{Z}e^{-\beta H_0}\\ (\langle\psi_n|\,A(\mathbf{Q},t)\,|\psi_m\rangle\,\langle\psi_m|\,B(-\mathbf{Q},t')\,|\psi_n\rangle - \langle\psi_n|\,B(-\mathbf{Q},t')\,|\psi_m\rangle\,\langle\psi_m|\,A(\mathbf{Q},t)\,|\psi_n\rangle)\end{aligned} \tag{A.32}$$

and by swapping n and m in the second term

$$\begin{aligned}\chi_{AB}(\mathbf{Q},\omega) = i\int_0^\infty d(t-t')e^{i\omega(t-t')}\frac{1}{V}\sum_{mn}\frac{1}{Z}\\ \Big(e^{-\beta E_n}\,\langle\psi_n|\,A(\mathbf{Q},t)\,|\psi_m\rangle\,\langle\psi_m|\,B(-\mathbf{Q},t')\,|\psi_n\rangle -\\ e^{-\beta E_m}\,\langle\psi_n|\,A(\mathbf{Q},t)\,|\psi_m\rangle\,\langle\psi_m|\,B(-\mathbf{Q},t')\,|\psi_n\rangle\Big) =\\ i\int_0^\infty d(t-t')e^{i\omega(t-t')}\frac{1}{V}\sum_{mn}\frac{1}{Z}\\ \langle\psi_n|\,A(\mathbf{Q},t)\,|\psi_m\rangle\,\langle\psi_m|\,B(-\mathbf{Q},t')\,|\psi_n\rangle\left(e^{-\beta E_n}-e^{-\beta E_m}\right) =\\ i\int_0^\infty d(t-t')e^{i\omega(t-t')}\frac{1}{V}\sum_{mn}\frac{e^{-\beta E_n}}{Z}\\ \langle\psi_n|\,A(\mathbf{Q},t)\,|\psi_m\rangle\,\langle\psi_m|\,B(-\mathbf{Q},t')\,|\psi_n\rangle\left(1-e^{-\beta(E_m-E_n)}\right).\end{aligned} \tag{A.33}$$

If the time dependencies of A and B are now written out explicitly, we get

$$\begin{aligned}\chi_{AB}(\mathbf{Q},\omega) = i\int_0^\infty d(t-t')e^{i\omega(t-t')}\frac{1}{V}\sum_{mn}\frac{e^{-\beta E_n}}{Z}\\ \langle\psi_n|\, e^{iH_0t}A(\mathbf{Q})e^{-iH_0t}\,|\psi_m\rangle\,\langle\psi_m|\, e^{iH_0t'}B(-\mathbf{Q})e^{-iH_0t'}\,|\psi_n\rangle\left(1-e^{-\beta(E_m-E_n)}\right) =\\ i\int_0^\infty d(t-t')e^{i\omega(t-t')}\frac{1}{V}\sum_{mn}\frac{e^{-\beta E_n}}{Z}e^{i(E_n-E_m)(t-t')}\\ \langle\psi_n|\, A(\mathbf{Q})\,|\psi_m\rangle\,\langle\psi_m|\, B(-\mathbf{Q})\,|\psi_n\rangle\left(1-e^{-\beta(E_m-E_n)}\right)\end{aligned} \tag{A.34}$$

and by using $\int_0^\infty e^{i\omega'(t-t')}d(t-t') = \frac{i}{\omega'+i\delta}$, where δ is an infinitesimally small positive constant, we get

$$\chi_{AB}(\mathbf{Q},\omega) = -\frac{1}{V}\sum_{mn}\frac{e^{-\beta E_n}}{Z}\,\langle\psi_n|\, A(\mathbf{Q})\,|\psi_m\rangle\,\langle\psi_m|\, B(-\mathbf{Q})\,|\psi_n\rangle\,\frac{1-e^{-\beta(E_m-E_n)}}{\omega-E_m+E_n+i\delta}. \tag{A.35}$$

The term $i\delta$ in the denominator of the expression for $\chi_{AB}(\mathbf{Q},\omega)$ makes the function analytical in the upper half plane while there is a pole in the lower half plane. This property ensures that, when doing the inverse Fourier transform

$$\chi_{AB}(\mathbf{Q},t) = \int_{-\infty}^\infty \frac{d\omega}{2\pi}\chi_{AB}(\mathbf{Q},\omega)e^{-i\omega t}, \tag{A.36}$$

$\chi_{AB}(\mathbf{Q},t)$ disappears for $t<0$ just as it should.

Looking at the correlation function, K, of two operators A and B, defined through

$$K_{AB}(\mathbf{x}-\mathbf{x}',t-t') = \langle A(\mathbf{x},t)B(\mathbf{x}',t')\rangle, \tag{A.37}$$

its Fourier transform is given by

$$K_{AB}(\mathbf{Q},\omega) = \frac{1}{V}\int_{-\infty}^\infty \langle A(\mathbf{Q},t)B(-\mathbf{Q},t')\rangle e^{i\omega(t-t')}d(t-t') \tag{A.38}$$

where one should note that correlations are invariant under inversion in a homogeneous system, hence $K_{AB}(\mathbf{Q},\omega) = K_{AB}(-\mathbf{Q},\omega)$. By calculating the expectation value in a similar fashion as before one obtains

$$\begin{aligned}K_{AB}(\mathbf{Q},\omega) = \frac{1}{V}\int_{-\infty}^\infty d(t-t')e^{i\omega(t-t')}\sum_n\langle\psi_n|\,\rho_0 A(\mathbf{Q},t)B(-\mathbf{Q},t')\,|\psi_n\rangle =\\ \frac{1}{V}\int_{-\infty}^\infty d(t-t')e^{i\omega(t-t')}\sum_n\frac{e^{-\beta E_n}}{Z}\,\langle\psi_n|\, A(\mathbf{Q},t)B(-\mathbf{Q},t')\,|\psi_n\rangle =\\ \frac{1}{V}\int_{-\infty}^\infty d(t-t')e^{i\omega(t-t')}\sum_{mn}\frac{e^{-\beta E_n}}{Z}\,\langle\psi_n|\, A(\mathbf{Q},t)\,|\psi_m\rangle\,\langle\psi_m|\, B(-\mathbf{Q},t')\,|\psi_n\rangle =\\ \frac{1}{V}\int_{-\infty}^\infty d(t-t')e^{i\omega(t-t')}\sum_{mn}\frac{e^{-\beta E_n}}{Z}e^{i(E_n-E_m)(t-t')}\,\langle\psi_n|\, A(\mathbf{Q})\,|\psi_m\rangle\,\langle\psi_m|\, B(-\mathbf{Q})\,|\psi_n\rangle =\\ \frac{2\pi}{V}\sum_{mn}\frac{e^{-\beta E_n}}{Z}\,\langle\psi_n|\, A(\mathbf{Q})\,|\psi_m\rangle\,\langle\psi_m|\, B(-\mathbf{Q})\,|\psi_n\rangle\,\delta(\omega+E_n-E_m).\end{aligned} \tag{A.39}$$

Comparing this expression to the expression for the response function in Equation (A.35) yields the relation

$$\chi_{AB}(\mathbf{Q},\omega) = -\frac{1}{2\pi}\int_{-\infty}^{\infty} d\omega' \frac{K_{AB}(\mathbf{Q},\omega')}{\omega-\omega'+i\delta}\left(1-e^{-\beta\omega'}\right) \tag{A.40}$$

where the δ-function in the expression for K_{AB} sets $\omega' = E_m - E_n$.

Cases, where the operator B is the hermitian adjoint of the operator A, have the property that

$$\langle\psi_n| A(\mathbf{Q}) |\psi_m\rangle^* = \langle\psi_m| A^\dagger(-\mathbf{Q}) |\psi_n\rangle \tag{A.41}$$

implying

$$K_{AA^\dagger}(\mathbf{Q},\omega) = \frac{2\pi}{V}\sum_{mn}\frac{e^{-\beta E_n}}{Z}|\langle\psi_n| A(\mathbf{Q}) |\psi_m\rangle|^2\delta(\omega+E_n-E_m), \tag{A.42}$$

which is a real and positive quantity. By using the relation in Equation (A.40), $\chi_{AA^\dagger}(\mathbf{Q},\omega)$ can be expressed

$$\begin{aligned}\chi_{AA^\dagger}(\mathbf{Q},\omega) = -\frac{1}{2\pi}\int_{-\infty}^{\infty} d\omega' \frac{K_{AA^\dagger}(\mathbf{Q},\omega')}{\omega-\omega'+i\delta}\left(1-e^{-\beta\omega'}\right) = \\ -\frac{1}{2\pi}\int_{-\infty}^{\infty} d\omega' \frac{K_{AA^\dagger}(\mathbf{Q},\omega')(\omega-\omega'-i\delta)}{(\omega-\omega')^2}\left(1-e^{-\beta\omega'}\right).\end{aligned} \tag{A.43}$$

Looking only at the imaginary part yields the relation

$$\mathrm{Im}(\chi_{AA^\dagger}(\mathbf{Q},\omega)) = \frac{1}{2\pi}\int_{-\infty}^{\infty} d\omega' \frac{K_{AA^\dagger}(\mathbf{Q},\omega')\delta}{(\omega-\omega')^2}\left(1-e^{-\beta\omega'}\right) \tag{A.44}$$

where the factor $\frac{\delta}{(\omega-\omega')^2}$ works like a δ-function setting $\omega' = \omega$ and cancelling the π in the denominator when integrating over ω', resulting in the relation

$$K_{AA^\dagger}(\mathbf{Q},\omega) = \frac{2}{1-e^{-\beta\omega}}\mathrm{Im}(\chi_{AA^\dagger}(\mathbf{Q},\omega)). \tag{A.45}$$

This is a part of the so-called fluctuation-dissipation theorem.

B

The Dielectric Function and Its Relation to the Density-Density Response Function

This appendix follows Ref. [57], especially the beginning of chapter 29, quite closely and aims to give an introduction to the dielectric function, $\varepsilon(\mathbf{Q}, \omega)$, and its relation to the density-density response function.

When an isotropic material is exposed to an external electric field, $\mathbf{E}(\mathbf{x}, t)$, the expression for the electric displacement, $\mathbf{D}(\mathbf{x}, t)$, looks like

$$D_\alpha(\mathbf{x}, t) = \int d\mathbf{x}' \int_{-\infty}^{t} dt' \varepsilon_{\alpha\beta}(\mathbf{x} - \mathbf{x}', t - t') E_\beta(\mathbf{x}', t') \tag{B.1}$$

where summation over the repeated index β is implied and $\varepsilon_{\alpha\beta}$ is the so called permittivity tensor. By Fourier transforming both the spatial and temporal component the relation

$$D_\alpha(\mathbf{Q}, \omega) = \varepsilon_{\alpha\beta}(\mathbf{Q}, \omega) E_\beta(\mathbf{Q}, \omega) \tag{B.2}$$

can be obtained. Decomposing the electric field and the electric displacement field into components that are parallel and perpendicular to the direction of $\mathbf{Q}$ their relations can be written according to

$$\mathbf{D}_\parallel(\mathbf{Q}, \omega) = \varepsilon_\parallel(\mathbf{Q}, \omega) E_\parallel(\mathbf{Q}, \omega) \tag{B.3}$$
$$\mathbf{D}_\perp(\mathbf{Q}, \omega) = \varepsilon_\perp(\mathbf{Q}, \omega) E_\perp(\mathbf{Q}, \omega) \tag{B.4}$$

where the dielectric function $\varepsilon_r(\mathbf{Q}, \omega)$ is defined as

$$\varepsilon_r(\mathbf{Q}, \omega) = \varepsilon_\parallel(\mathbf{Q}, \omega). \tag{B.5}$$

When an external charge density, $\rho_{\text{ext}}(\mathbf{x}, t)$, is introduced into an originally homogeneous electron gas, it can be related to the electric displacement, $\mathbf{D}(\mathbf{x}, t)$, via Gauss's law

$$\nabla \cdot \mathbf{D}(\mathbf{x}, t) = \rho_{\text{ext}}(\mathbf{x}, t). \tag{B.6}$$

The coulomb interactions of the external charges and the electrons of the system induce a redistribution of the electrons in the originally homogeneous system leading to an induced charge density $\rho_{\text{ind}}(\mathbf{x}, t)$. The electric field, $\mathbf{E}(\mathbf{x}, t)$, is related to the total charge density

$$\rho(\mathbf{x}, t) = \rho_{\text{ext}}(\mathbf{x}, t) + \rho_{\text{ind}}(\mathbf{x}, t) \tag{B.7}$$

via

$$\nabla \cdot \mathbf{E}(\mathbf{x}, t) = \rho(\mathbf{x}, t) \tag{B.8}$$

and the electric field is also related to the scalar potential, $\varphi(\mathbf{x}, t)$, through

$$\mathbf{E}(\mathbf{x}, t) = -\nabla\varphi(\mathbf{x}, t). \tag{B.9}$$

Analogously to this, an external potential, $\varphi_{\text{ext}}(\mathbf{x}, t)$, can be introduced and relates to the electric displacement through

$$\mathbf{D}(\mathbf{x}, t) = -\nabla\varphi_{\text{ext}}(\mathbf{x}, t). \tag{B.10}$$

Taking the Fourier transform of these expressions leads to

$$\mathbf{E}(\mathbf{Q}, \omega) = -i\mathbf{Q}\varphi(\mathbf{x}, t) \tag{B.11}$$
$$\mathbf{D}(\mathbf{Q}, \omega) = -i\mathbf{Q}\varphi_{\text{ext}}(\mathbf{x}, t) \tag{B.12}$$

implying that $\mathbf{E} = \mathbf{E}_{\|}$, $\mathbf{D} = \mathbf{D}_{\|}$ and that, from Equation (B.3),

$$\varphi(\mathbf{Q}, \omega) = \frac{\varphi_{\text{ext}}(\mathbf{Q}, \omega)}{\varepsilon_r(\mathbf{Q}, \omega)}. \tag{B.13}$$

Furthermore, substituting equations (B.9) and (B.10) into equations (B.8) and (B.6) leads to

$$\nabla^2\varphi(\mathbf{x}, t) = -\rho(\mathbf{x}, t) \tag{B.14}$$
$$\nabla^2\varphi_{\text{ext}}(\mathbf{x}, t) = -\rho_{\text{ext}}(\mathbf{x}, t) \tag{B.15}$$

or equivalently, in terms of their Fourier transforms,

$$Q^2\varphi(\mathbf{Q}, \omega) = \rho(\mathbf{Q}, \omega) \tag{B.16}$$
$$Q^2\varphi_{\text{ext}}(\mathbf{Q}, \omega) = \rho_{\text{ext}}(\mathbf{Q}, \omega). \tag{B.17}$$

Using the relation from Equation (B.13) in Equation (B.16) leads to

$$Q^2\frac{\varphi_{\text{ext}}(\mathbf{Q}, \omega)}{\varepsilon_r(\mathbf{Q}, \omega)} = \rho(\mathbf{Q}, \omega) \implies \varphi_{\text{ext}}(\mathbf{Q}, \omega) = \frac{\varepsilon_r(\mathbf{Q}, \omega)\rho(\mathbf{Q}, \omega)}{Q^2} \tag{B.18}$$

and by putting this into Equation (B.17) it becomes

$$\varepsilon_r(\mathbf{Q}, \omega)\rho(\mathbf{Q}, \omega) = \rho_{\text{ext}}(\mathbf{Q}, \omega) \implies \rho(\mathbf{Q}, \omega) = \frac{\rho_{\text{ext}}(\mathbf{Q}, \omega)}{\varepsilon_r(\mathbf{Q}, \omega)}. \tag{B.19}$$

By now expressing ρ in terms of ρ_{ext} and ρ_{ind} according to Equation (B.7), the above expression becomes

$$\frac{1}{\varepsilon_r(\mathbf{Q}, \omega)} = 1 + \frac{\rho_{\text{ind}}(\mathbf{Q}, \omega)}{\rho_{\text{ext}}(\mathbf{Q}, \omega)} \tag{B.20}$$

and using Equation (B.17) it can be rewritten

$$\frac{1}{\varepsilon_r(\mathbf{Q},\omega)} = 1 + \frac{1}{Q^2}\frac{\rho_{\text{ind}}(\mathbf{Q},\omega)}{\varphi_{\text{ext}}(\mathbf{Q},\omega)}. \tag{B.21}$$

Redefining the charge density to coincide with the notation used in the rest of this thesis $\rho_i \to e\rho_i$, meaning ρ is now rather the electron number density, and defining the electric potential $U_i \equiv \varphi_i e$, the above expression becomes

$$\frac{1}{\varepsilon_r(\mathbf{Q},\omega)} = 1 + \frac{e^2}{Q^2}\frac{\rho_{\text{ind}}(\mathbf{Q},\omega)}{U_{\text{ext}}(\mathbf{Q},\omega)} \tag{B.22}$$

where $\frac{\rho_{\text{ind}}(\mathbf{Q},\omega)}{U_{\text{ext}}(\mathbf{Q},\omega)} \equiv \chi_{\rho\rho}(\mathbf{Q},\omega)$ is the density-density response function that is used heavily in this thesis.

To tie it together with the discussion in the appendix about linear response theory, Appendix A, the density-density response function is given by

$$\chi_{\rho\rho}(\mathbf{x},\mathbf{x}',t-t') = -i\theta(t-t')\langle[\rho(\mathbf{x},t),\rho(\mathbf{x}',t')]\rangle \tag{B.23}$$

where the extra minus sign in this expression compared to Equation (A.27) comes from the definition of the perturbing Hamiltonian

$$H_{\text{ext}}(t) = \int d\mathbf{x}\rho(\mathbf{x})U_{\text{ext}}(\mathbf{x},t), \tag{B.24}$$

which differs by a minus sign compared to the perturbing Hamiltonian in Equation (A.1). Also, the correlation function, $K_{\rho\rho}$, can be defined, and both the density-density response function and the correlation function can be Fourier transformed into the momentum and frequency domain as in Appendix A. The Fourier transform of the correlation function can, in this context, also be called the dynamic structure factor, $S(\mathbf{Q},\omega)$. Via the fluctuation-dissipation theorem presented at the end of Appendix A the dynamic structure factor and the density-density response function can be related through

$$S(\mathbf{Q},\omega) = -\frac{2}{1-e^{-\beta\omega}}\text{Im}(\chi_{\rho\rho}(\mathbf{Q},\omega)). \tag{B.25}$$

C

Solar Model

The solar model used in this thesis comes from Ref. [58]. By using it, the radially dependent values for the electron number density, $n_e(r)$, the temperature, $T(r)$, and mass profile, $M_\odot(r)$, can be obtained. Furthermore from equation (3.10) the radially dependent escape velocity, $v_{\text{esc}}(r)$, can also be calculated. In Figure C.1 the different properties are plotted as a function of the radial position using $M_\odot = 2 \cdot 10^{30}$ kg, $T(0) = 1.6 \cdot 10^7$ K, $v_{\text{esc}}(0) = 0.0046$ and $n_e(0) = 6 \cdot 10^{25}$ cm^{-3}.

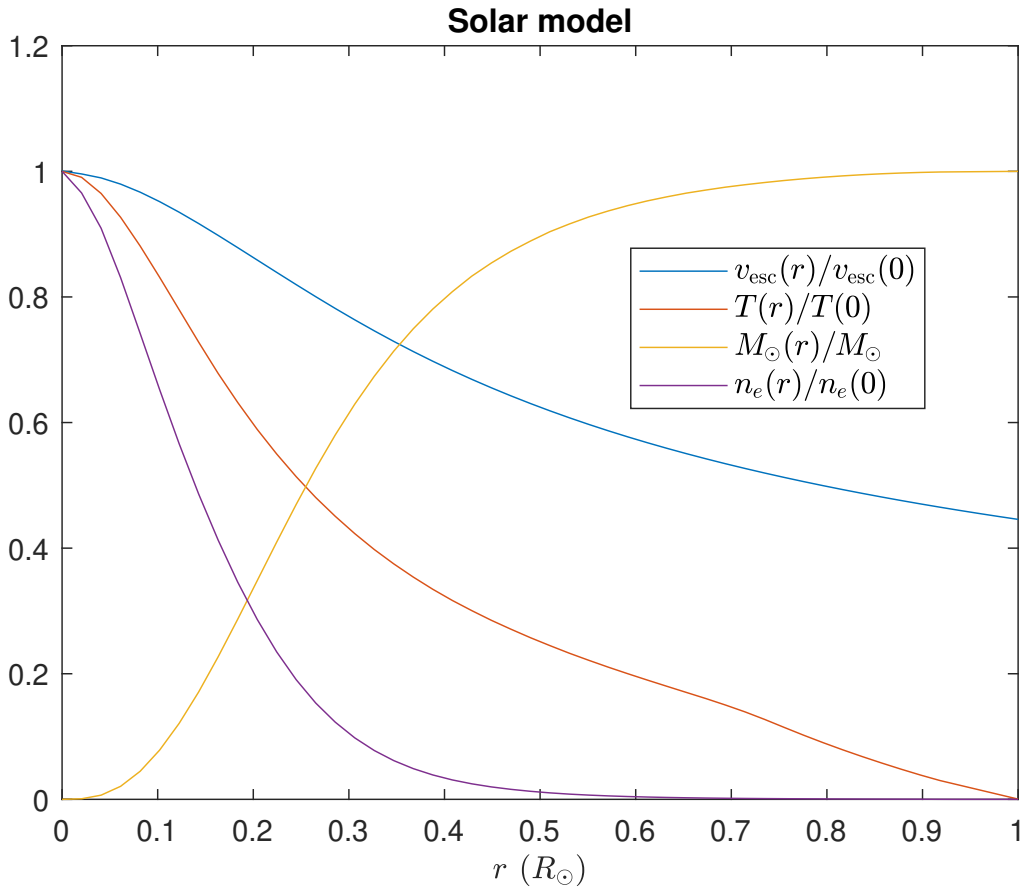

Figure C.1: Plot of the escape velocity, temperature, mass profile and electron number density as a function of the radius inside the Sun.

DEPARTMENT OF PHYSICS
CHALMERS UNIVERSITY OF TECHNOLOGY
Gothenburg, Sweden
www.chalmers.se

CHALMERS
UNIVERSITY OF TECHNOLOGY